

Scalable and Efficient Continual Learning from Demonstration via Hypernetwork-generated Stable Dynamics Model

Sayantan Audyy*, Jakob Hollenstein*, Matteo Saveriano†, Antonio Rodríguez-Sánchez*, Justus Piater*‡

* Department of Computer Science, University of Innsbruck, Austria

† Department of Industrial Engineering, University of Trento, Italy

‡ Digital Science Center (DiSC), University of Innsbruck, Austria

Abstract—Learning from demonstration (LfD) provides an efficient way to train robots. The learned motions should be convergent and stable, but to be truly effective in the real world, LfD-capable robots should also be able to remember multiple motion skills. Multi-skill retention is a capability missing from existing stable-LfD approaches. On the other hand, recent work on continual-LfD has shown that hypernetwork-generated neural ordinary differential equation solvers, can learn multiple LfD tasks sequentially, but this approach lacks stability guarantees. We propose an approach for *stable continual-LfD* in which a hypernetwork generates *two* networks: a *trajectory learning* dynamics model, and a *trajectory stabilizing* Lyapunov function. The introduction of stability not only generates stable trajectories but also greatly improves continual learning performance, especially in the size-efficient *chunked hypernetworks*. With our approach, we can continually train a single model to predict the position and orientation trajectories of the robot’s end-effector simultaneously for multiple real world tasks without retraining on past demonstrations. We also propose *stochastic regularization* with a *single* randomly sampled regularization term in hypernetworks, which reduces the cumulative training time cost for N tasks from $\mathcal{O}(N^2)$ to $\mathcal{O}(N)$ without any loss in performance in real-world tasks. We empirically evaluate our approach on the popular LASA dataset, on high-dimensional extensions of LASA (including up to 32 dimensions) to assess scalability, and on a novel extended robotic task dataset (RoboTasks9) to assess real-world performance. In trajectory error metrics, stability metrics and continual learning metrics our approach performs favorably, compared to other baselines. Code and datasets will be shared after submission¹.

Index Terms—Learning from demonstration, continual learning, hypernetworks.

I. INTRODUCTION

Learning from demonstration (LfD) is a natural way for humans to impart movement skills to robots. Robots trained with LfD are required to not only reproduce the motions demonstrated by the human user, but also to guarantee the stability of the produced motion [1]. Methods employed for LfD must be able to generalize to different initial conditions, make sure that the robot’s trajectory does not diverge, and that the robot does not assume unsafe configurations during its motion. Accordingly, the focus of recent LfD techniques [2]–[6] has been on ensuring that these required stability and convergence

properties are satisfied. However, these LfD methods focus on learning only a single motion skill. Consequently, to learn a new skill the robot must be retrained from scratch and the previously learned skill is forgotten. Recent work in *continual LfD* [7] has shown that a system of *neural ordinary differential equation solvers* (NODEs) [8] and *hypernetworks* [9], [10] can continually learn and remember a sequence of motion skills without the need of retraining on past demonstrations. However, this approach has limitations such as lack of stability of the learned vector field, degrading performance for long task sequences, and increase in hypernetwork training time for each additional task. In the current paper we overcome these limitations which are critical for a robot in the real world.

We propose a novel continual-LfD system in which a hypernetwork generates the parameters of our proposed time-dependent *stable NODE* (*sNODE*) that is composed of *two* neural networks: (i) a network that represents a nominal dynamics model, and (ii) an additional network that parameterizes a *Lyapunov function* that is responsible for ensuring the stability of the predicted trajectories.

Our proposed continual-LfD system is able to learn and remember long sequences of trajectory learning tasks without storing or retraining on the data of past tasks. It produces stable, non-divergent trajectory predictions that eliminate the possibility of robot movements which are dangerous for humans in the vicinity of the robot or for the robot itself. Most importantly, we show that the introduction of stability leads to much improved continual learning performance compared to the non-stable alternative. This improvement is most prominent for *chunked hypernetworks* [7], that are smaller hypernetworks that produce the parameters of the target networks in smaller segments called *chunks*. With our proposed approach, these limited capacity hypernetworks are able to remember a long sequence of tasks, even for high-dimensional trajectory-learning tasks. In experiments involving real world tasks, we propose a single model that can predict both the position and orientation of the robot’s end-effector simultaneously. In contrast to using separate models for position and orientation, our approach roughly halves the number of required model parameters without compromising on performance. We propose a stochastic regularization approach for hypernetworks in which a *single* randomly sampled regularization term is added to the optimization objective instead of adding a regularization term

Corresponding author: sayantan.auddy@uibk.ac.at

¹This paper is currently under internal review.

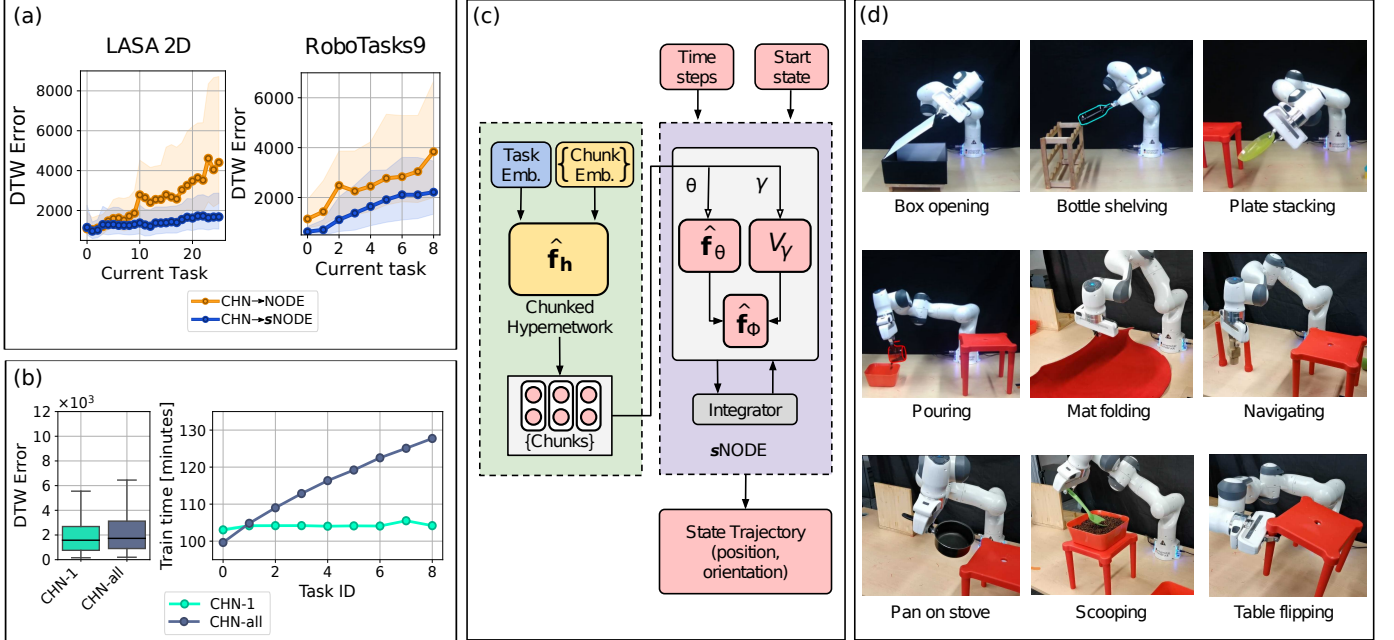


Fig. 1. Overview of key results and our proposed approach. (a) Continual learning from demonstration with stable NODEs generated by a chunked hypernetwork (CHN \rightarrow sNODE) outperforms NODE-based continual learning (CHN \rightarrow NODE) by a wide margin (details in Sec. VI). (b) Stochastic regularization with a single regularization term (CHN-1) leads to a CHN \rightarrow sNODE model that performs as well as the fully regularized model (CHN-all) but reduces the training cost of N real-world tasks from $\mathcal{O}(N^2)$ to $\mathcal{O}(N)$ (details in Sec. VI). (c) Architecture of a CHN \rightarrow sNODE model: task-specific learned parameters are shown in \blacksquare , regularized (task-independent) parameters are shown in \blacksquare , and non-trainable inputs/outputs are shown in \blacksquare (details in Sec. IV). (d) Illustrations of the nine real-world tasks of the RoboTasks9 dataset proposed by us. The last 5 tasks are introduced in this paper (details in Sec. V). With our proposed approach, all tasks can be learned in a continual manner with a single model without retraining on past demonstrations, with minimal forgetting, and with stability in the predicted trajectories.

for each past task. With this approach, the cumulative training cost is reduced from $\mathcal{O}(N^2)$ to $\mathcal{O}(N)$ in the number of tasks N , without any impact on performance in real-world tasks.

We perform experiments on the popular LASA trajectory learning dataset [11], that contains 26 tasks [7] of 2-dimensional trajectories. To evaluate the scalability of our approach to higher dimensions, we create high-dimensional analogues of the LASA dataset. We combine multiple tasks from the original LASA dataset to create new datasets of 8-, 16-, and 32-dimensional trajectories. Each of these new datasets contain 10 tasks each. We add 5 new tasks to the *RoboTasks* dataset [7], creating a new dataset RoboTasks9 containing 9 real-world LfD tasks. For all datasets (LASA 2D, LASA 8D, LASA 16D, LASA 32D, and RoboTasks9), we evaluate our hypernetwork \rightarrow sNODE models against all major groups of continual learning methods (*replay*, *dynamic architectures*, and *regularization*) [12], as well as against the models using NODE proposed in [7]. We report quantitative metrics for the accuracy of predicted trajectories, as well as for the continual learning performance. We also report stability metrics. Additionally, we evaluate our approach qualitatively on a Franka Emika Panda robot in the real world. An overview of our approach and key results are shown in Fig. 1.

Our contributions can be summarized as follows:

- We propose an approach for *stable, continual* learning from demonstration with hypernetworks and sNODE that not only remembers multiple trajectory learning tasks and produces stable trajectories, but also improves the continual learning performance of the system compared

to the non-stable alternative.

- We improve the accuracy of the sNODE model by introducing a time input.
- We propose a single hypernetwork \rightarrow sNODE model that learns multiple tasks continually and predicts position and orientation trajectories simultaneously for real-world tasks.
- We introduce a form of stochastic hypernetwork regularization with a *single* randomly sampled regularization term that reduces the cumulative training cost for N tasks from $\mathcal{O}(N^2)$ to $\mathcal{O}(N)$.
- We create high-dimensional versions of the LASA dataset, and extend the RoboTasks dataset [7] by adding 5 new real-world tasks to create RoboTasks9.

II. RELATED WORK

Robot learning from demonstration (LfD) is a means for humans to teach motion skills to robots without explicitly programming them [13], which allows even users without expertise in robotics to train robots. It is also known by other names such as *programming by demonstration* or *imitation learning* [13], [14]. The demonstrations required for training robots via LfD can be obtained by different means, some of which are: (i) using a motion-tracking system to record human motions, (ii) using teleoperation to operate the robot while recording the robot's state, or (iii) using kinesthetic teaching where a human user physically guides the robot to perform a motion task [13], [15]–[17]. Once the demonstrations are available, there exist several different algorithmic approaches

for learning from this data [13]. Supervised learning has been used to learn from either a single demonstration [18] or a collection of demonstrations [19]. LfD has also been used in conjunction with reinforcement learning (RL) [20] where RL is used to refine the skills learned with LfD. Another approach is to learn a cost function from demonstrations and then to train a model predictive controller to reproduce the skills through inverse RL [21] or through constrained optimization [22]. In addition to demonstrations which show the robot the motion it has to perform, negative demonstrations have also been shown to be advantageous [23]. We refer the reader to [13], [15], [16] for a comprehensive overview of LfD.

In this paper, we focus on a subfield of LfD: *trajectory-based* learning methods that use a supervised approach for acquiring motion skills. These methods can be broadly categorized into two groups [17]:

some methods use *generative models* to fit a distribution from the training data [2], [3], [11], while other methods exploit *function approximators* like neural networks to fit the training data [6], [24]. In both groups, training data can be used to learn a *static mapping* (time input \rightarrow desired position) or a *dynamic mapping* (input position \rightarrow desired velocity). A dynamic mapping generates vector fields where input quantities are transformed into their time derivatives, and different strategies have been proposed to ensure convergence of the vector field to a given target [2], [4]–[6]. Among others, the *Imitation Flow* (iFlow) approach of Urain et al. [2] leverages the representational power of neural networks and normalizing flows to learn vector fields from demonstrations. Another neural network based approach for learning vector fields is *Neural Ordinary Differential Equation solvers* (NODEs) [8]. In [7], NODEs are used to learn LfD tasks in the real world. Manek and Kolter [6] present an approach for learning stable deep dynamics models by jointly learning a nominal dynamics model (similar to a NODE) and a *Lyapunov* function parameterized by an Input Convex Neural Network (ICNN). However, the authors of [6] do not conduct any robotics experiments.

Trajectory-based LfD is a mature research field, but most methods assume that different tasks are encoded in different representations, i.e., one has to fit a new model for each task the robot has to execute [13]. In this paper, we take the continual learning perspective on learning by demonstration and propose an approach capable of continuously learning new tasks, while producing stable trajectory predictions and without needing to store and use the training data from past tasks.

Continual Learning approaches in the current literature mostly address the problem of continual image classification. Popular strategies include growing the network architecture [25], replaying data from past tasks, or regularizing trainable parameters to avoid catastrophic forgetting [12]. *Replay*-based methods cache samples of real data from past tasks [26], or use generative models to create pseudo-samples of past data [27], which are interleaved with the current task's data during training. *Regularization*-based methods [28], [29] add a regularization term to the learning objective to minimize changes to parameters important for solving previous tasks. Refer to [12], [30] for in-depth surveys on continual learning methods.

Continual learning has also been successfully applied to robotics, though the number of such studies is relatively few. Gao et al. [31] present an approach for continual imitation learning that relies on deep generative replay [27] and action-conditioned video prediction to generate state and action trajectories of past tasks. This pseudo-data is interleaved with demonstrations of the current task to train a policy network that controls the robot's actions. The authors note that the generation of high-quality video frames can be problematic for a long sequence of tasks.

Xie and Finn [32] propose a method for lifelong robotic reinforcement learning that seeks to improve the forward transfer performance while learning a new current task by pre-training on the entire experience collected from all previous tasks. The problem of catastrophic forgetting is not considered.

Huang et al. [33] continually learn a dynamics model for reinforcement learning. In their work, a task-conditioned hypernetwork generates the parameters of the dynamics model for reinforcement learning tasks such as opening doors or pushing blocks. In contrast, we use hypernetworks for generating parameters for a trajectory learning *stable* NODE in a setup for learning from demonstration. We follow a supervised approach and do not need to rely on robot simulators. Compared to [33], we evaluate on much longer sequences of tasks and also investigate the effectiveness of chunked hypernetworks [10]. In addition, we qualitatively evaluate our approach on a physical robot. A hypernetwork solution for supervised continual-LfD is also proposed in [7], where the parameters of a NODE are generated with a hypernetwork. In this paper, we generate the parameters of a stable NODE (which comprises two different neural networks) with a hypernetwork. We compare our proposed models against [7] and achieve much better performance. Our approach has guarantees regarding the stability of the predicted robot trajectories. We also propose a solution for the training time growth of hypernetworks. In [7], the highest dimension of the trajectories used for evaluation is 3 compared to 32 in this paper. Finally, for real world robot tasks our models predict position and orientation trajectories simultaneously, and we train and evaluate our models on a sequence of 9 tasks, whereas in [7], only 4 real world tasks are learned.

LfD involves learning the entire vector field of a robot's motion from only a handful of demonstration trajectories. This makes it a more challenging problem than typical supervised regression or classification scenarios where the amount of training data is usually much greater. To continually learn such vector fields of different kinds of motion demonstrations and predict stable trajectories, we need to tackle the challenges of stable-LfD as well as the problem of *catastrophic forgetting* associated with neural networks. To the best of our knowledge, ours is the first work that demonstrates that continual stable-LfD is feasible for sequences of real-world robot tasks.

III. BACKGROUND

The continual-LfD models and baselines in this paper are composed of two subsystems: (i) a *learning from demonstration* (LfD) system that learns motion skills from demonstration, and

(ii) a *continual learning* system that mitigates *catastrophic forgetting* when multiple motion skills are learned. In this section, we briefly describe the fundamentals of these subsystems.

A. Learning from Demonstration

In this paper, we focus on neural network based continual learning. Hence, we consider neural network-based approaches for learning trajectories of the robot's end-effector position and orientation from human demonstrations.

1) *Neural ODEs and Stability*: A Neural Ordinary Differential Equation solver (NODE) [8] is a neural network that learns a dynamical system directly from observations. In this approach, a fully-connected neural network $\hat{\mathbf{f}}_\theta(\mathbf{x}) : \mathbb{R}^n \rightarrow \mathbb{R}^n$ with parameters θ represents a dynamical system. By integrating this function over time, an approximate solution to the ODE system at time t can be obtained as

$$\hat{\mathbf{x}}_t = \hat{\mathbf{x}}_0 + \int_0^t \hat{\mathbf{f}}_\theta(\hat{\mathbf{x}}_\tau) d\tau \quad (1)$$

where $\hat{\mathbf{x}}_0$ is the start of the trajectory. If we have a dataset \mathcal{D} of N observed trajectories $\{\mathbf{x}_{0:T-1}^{(0)}, \dots, \mathbf{x}_{0:T-1}^{(N-1)}\}$, where each trajectory $\mathbf{x}_{0:T-1}^{(i)}$ is a sequence of T points $\mathbf{x}_t^{(i)} \in \mathbb{R}^d$. The parameters θ can be learned using the dataset \mathcal{D} by minimizing the following loss [7]:

$$\mathcal{L} = \frac{1}{2} \sum_t \|\mathbf{x}_t - \hat{\mathbf{x}}_t\|_2^2 \quad (2)$$

A basic NODE trained by minimizing Eq. (2) does not provide any formal guarantees regarding the stability of the predicted trajectories. If the learning is not successful or if the starting state of the trajectory is different from the demonstrations, then it is possible for the predicted trajectory to diverge from the goal. This can be dangerous when such a system is used to control a robot.

To solve this problem, Manek and Kolter [6] propose to jointly learn a dynamics model and a *Lyapunov* function that ensures stability. In addition to the nominal dynamics model $\hat{\mathbf{f}}_\theta(\mathbf{x}) : \mathbb{R}^n \rightarrow \mathbb{R}^n$, let $V_\gamma(\mathbf{x}) : \mathbb{R}^n \rightarrow \mathbb{R}$ (parameterized by γ) denote a Lyapunov function, which is a positive definite function, such that $V_\gamma(\mathbf{x}) \geq 0$ for $\mathbf{x} \neq 0$ and $V_\gamma(0) = 0$. The projection of $\hat{\mathbf{f}}_\theta$ which satisfies the following condition

$$\nabla V_\gamma(\mathbf{x})^T \hat{\mathbf{f}}_\theta(\mathbf{x}) \leq -\alpha V_\gamma(\mathbf{x}) \quad (3)$$

ensures a stable dynamics system, where $\alpha \geq 0$ is a constant. The following function is guaranteed to produce stable trajectories [6]:

$$\begin{aligned} \mathbf{f}_\phi(\mathbf{x}) &= \text{Proj} \left(\hat{\mathbf{f}}_\theta(\mathbf{x}), \{f : \nabla V_\gamma(\mathbf{x})^T f(\mathbf{x}) \leq -\alpha V_\gamma(\mathbf{x})\} \right) \\ &= \hat{\mathbf{f}}_\theta(\mathbf{x}) - \nabla V_\gamma(\mathbf{x}) \frac{\text{ReLU}(\nabla V_\gamma(\mathbf{x})^T \hat{\mathbf{f}}_\theta(\mathbf{x})) + \alpha V_\gamma(\mathbf{x})}{\|\nabla V_\gamma(\mathbf{x})\|_2^2} \end{aligned} \quad (4)$$

where $\phi = \{\theta, \gamma\}$ represents the parameters of the nominal dynamics model and the Lyapunov function taken together. The Lyapunov function V_γ is modeled with an input-convex neural network (ICNN) [34]. During training, both the parameters of

the nominal dynamics model $\hat{\mathbf{f}}_\theta(\mathbf{x})$ and the Lyapunov function V_γ are learned jointly [6] with Eq. (2). In the rest of this paper, we refer to the stable dynamics model represented by Eq. (4) as *stable NODE* (*sNODE*).

2) *Learning Orientation Trajectories*: The orientation of the robot's end-effector is often encoded with unit quaternions. Since a trajectory of orientations does not lie in Euclidean space, we follow the same approach as [7], [35], [36] and project quaternions into the tangent space, which is a local Euclidean space.

Consider a trajectory of quaternions $\mathbf{q}_{0:T-1}$ comprising of a sequence of T quaternions, in which each quaternion $\mathbf{q}_t = [v_t^{(i)}, \mathbf{u}_t^{(i)}]^T$, where $\mathbf{q}_t \in \mathbb{S}^3$, $v_t \in \mathbb{R}$ and $\mathbf{u}_t \in \mathbb{R}^3$. Each quaternion $\mathbf{q}_t \in \mathbb{S}^3$ in the trajectory $\{\mathbf{q}_0, \dots, \mathbf{q}_t, \dots, \mathbf{q}_{T-1}\}$ can be projected into its corresponding rotation vector $\mathbf{r}_t \in \mathbb{R}^3$ in the tangent space using the *logarithmic map* [37] $\text{Log}(\cdot) : \mathbb{S}^3 \mapsto \mathbb{R}^3$:

$$\begin{aligned} \mathbf{r}_t &= \text{Log}(\bar{\mathbf{q}}_t * \mathbf{q}_{T-1}) \\ \text{where } \text{Log}(\mathbf{q}) &= \begin{cases} \arccos(v) \frac{\mathbf{u}}{\|\mathbf{u}\|} & \text{if } \|\mathbf{u}\| > 0, \\ [0, 0, 0]^T & \text{otherwise.} \end{cases} \end{aligned} \quad (5)$$

The transformed trajectory in the tangent space can be learned with the help of Eq. (4) and Eq. (2). After the trajectories of rotation vectors have been learned, the model's predictions are also in the form of rotation vector trajectories. Each rotation vector $\hat{\mathbf{r}}_t \in \mathbb{R}^3$ in a predicted trajectory $\{\hat{\mathbf{r}}_0, \dots, \hat{\mathbf{r}}_t, \dots, \hat{\mathbf{r}}_{T-1}\}$ can be projected back to a corresponding quaternion $\hat{\mathbf{q}}_t \in \mathbb{S}^3$ on the hypersphere using the *exponential map* [37] $\text{Exp}(\cdot) : \mathbb{R}^3 \mapsto \mathbb{S}^3$:

$$\begin{aligned} \hat{\mathbf{q}}_t &= \mathbf{q}_{T-1} * \text{Exp}(\hat{\mathbf{r}}_t) \\ \text{where } \text{Exp}(\mathbf{r}) &= \begin{cases} \left[\cos(\|\mathbf{r}\|), \sin(\|\mathbf{r}\|) \frac{\mathbf{r}^T}{\|\mathbf{r}\|} \right]^T & \text{if } \|\mathbf{r}\| > 0, \\ [1, 0, 0, 0]^T & \text{otherwise.} \end{cases} \end{aligned} \quad (6)$$

Similar to [7], [35], [36], we assume that the input domain of $\text{Log}(\cdot)$ is restricted to \mathbb{S}^3 except for $[1, 0, 0, 0]^T$ and the input domain of $\text{Exp}(\cdot)$ satisfies $\|\zeta\| < \pi$.

B. Continual Learning

We consider continual learning approaches from all the major families of methods in the literature [12], [30]: *dynamic architectures* (new parameters are added for each new task), *replay* (past training data is stored and reused while learning a new task), and *regularization* (parameters are protected from catastrophic forgetting using regularization while learning a new task). In this section, we briefly describe the continual learning methods that are related to our proposed methods and experimental baselines.

1) *Dynamic Architectures*: A straightforward approach to continual learning is to increase the capacity of the model to learn new tasks. This can be done by learning each task with a separate network [25], or by using a dynamic architecture to only add as many parameters as needed [38], [39].

2) *Replay*: A portion of the training data (or the entire data) for each task is stored, and for every new task, the cached data from past tasks is combined with the data of the current task to train a model [7].

3) *Regularization*: Regularization-based continual learning methods append additional components to the optimization objective for learning each new task. These methods can be divided into two groups: (i) direct regularization, and (ii) meta-model regularization.

a) *Direct Regularization*: To prevent changes to the network parameters that are *important* for solving previous tasks, a weighted L2 regularization term is added to the learning objective. Typically, the loss $\tilde{\mathcal{L}}^m$ for the m^{th} task takes the following form [7]:

$$\tilde{\mathcal{L}}^m = \mathcal{L}^m + c \sum_k \Omega_k^m (\theta_k^* - \theta_k)^2 \quad (7)$$

where \mathcal{L}^m is the task-specific loss (e.g. MSE loss, or cross-entropy loss, etc.), c denotes the regularization constant, and Ω_k^m is the importance of the k^{th} parameter for the m^{th} task. θ_k^* and θ_k represent the value of the k^{th} parameter before learning the current task and during the present iteration respectively. The distinguishable characteristic of these methods is that the parameters being regularized belong to the model that solves the task we are interested in (e.g. for an image classifying convolutional network, the parameters of the convolutional network are regularized directly). The different direct-regularization methods differ from each other in the way the importance term Ω_k^m is computed [28], [29], [40].

b) *Meta-model Regularization*: Instead of directly protecting the parameters of the model that learns the tasks under consideration, a meta-model, known as a *hypernetwork* [9], [10] is used to generate the parameters of the *task learning* model. The parameters of the hypernetwork are protected from catastrophic forgetting with regularization.

Consider that a hypernetwork with parameters \mathbf{h} generates the parameters θ^m of a task learner for the m^{th} task in a sequence of continual learning tasks. For optimizing \mathbf{h} , a two-stage process is followed [7], [10]. In the first stage, a candidate change $\Delta\mathbf{h}$ is determined such that the task-specific loss \mathcal{L}^m for the m^{th} task is minimized. The task-specific loss \mathcal{L}^m depends on the task-learner parameters θ^m (which are generated by the hypernetwork) and \mathbf{x}^m , the data for the m^{th} task. Thus,

$$\mathcal{L}^m = \mathcal{L}^m(\theta^m = \mathbf{f}(\mathbf{e}^m, \mathbf{h}), \mathbf{x}^m) \quad (8)$$

where \mathbf{f} represents the hypernetwork function and \mathbf{e}^m denotes the *task embedding vector* for the m^{th} task, that forms the input to the hypernetwork. In the second stage, the parameters \mathbf{h} and the task embedding vector \mathbf{e}^m are optimized by minimizing the regularized loss $\tilde{\mathcal{L}}^m$ [7], [10]:

$$\begin{aligned} \tilde{\mathcal{L}}^m = & \mathcal{L}^m(\theta^m = \mathbf{f}(\mathbf{e}^m, \mathbf{h}), \mathbf{x}^m) \\ & + \frac{\beta}{m-1} \sum_{l=0}^{m-1} \|\mathbf{f}(\mathbf{e}^l, \mathbf{h}^*) - \mathbf{f}(\mathbf{e}^l, \mathbf{h} + \Delta\mathbf{h})\|^2 \end{aligned} \quad (9)$$

Here, β denotes the regularization constant and \mathbf{h}^* denotes the hypernetwork parameters before learning the m^{th} task. For each task, a separate task embedding vector is learned and then frozen for regularizing the learning of future tasks.

Since the parameters θ^m of the task learner are produced from the final layer of the hypernetwork, the hypernetwork can

be quite large. To overcome this limitation, *chunked* hypernetworks have been proposed [10], in which the parameters θ^m are produced piecemeal in segments called *chunks*. In addition to the task embedding vector \mathbf{e}^m , chunked hypernetworks make use of additional inputs called *chunk embedding vectors*. Similar to the task embedding vectors, these chunk embedding vectors are also trainable. However, a separate task embedding vector is learned for each task, whereas a single set of chunk embedding vectors is shared across all tasks and is regularized in the same way as the parameters of the hypernetwork.

IV. METHODS

The continual-LfD approach proposed in this paper consists of two sub-systems: a stable node (*sNODE*) that learns the trajectories of each task, and a hypernetwork-based continual learning mechanism that makes it possible to learn multiple tasks without revisiting data from past tasks. In this section, we present the details of our approach that results in stable trajectory predictions, improved continual learning performance, and better scalability of training times.

A. Stable NODE with Time input

We introduce an additional time input to the *sNODE* model which results in more accurate trajectory predictions. Previously, it has been shown that the addition of a time input to a NODE enables it to learn a time-dependant vector field [41], thereby improving the accuracy of the predicted trajectories [7]. Motivated by this, we extend the *sNODE* model [6] by making it time-dependant, as shown in Fig. 2. This time input needs to be provided to the nominal dynamics model $\hat{\mathbf{f}}_\theta$, as well as to the Lyapunov function V_γ . Since the resultant dynamics model for *sNODE* emerges from the combination of $\hat{\mathbf{f}}_\theta$ and V_γ , the introduction of the time input is non-trivial.

We first concatenate the time input t with the state \mathbf{x}_t to create an augmented state $\hat{\mathbf{x}}_t = [\mathbf{x}_t, t]$. The input layer of the neural network representing the nominal dynamics model $\hat{\mathbf{f}}_\theta$ is

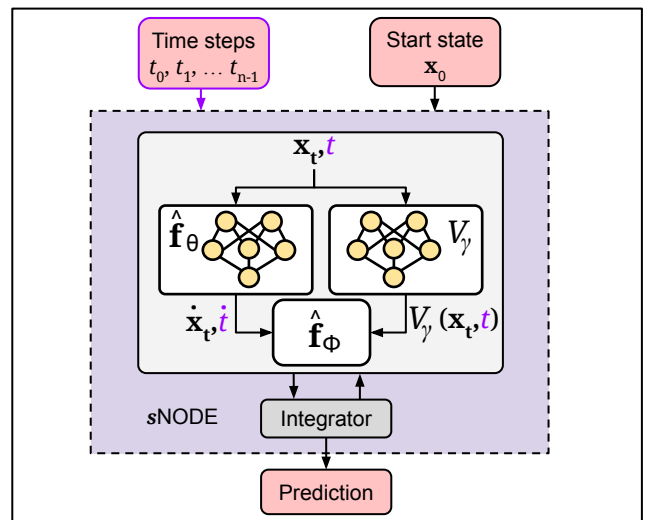


Fig. 2. Time dependent stable NODE (*sNODE*) architecture: time input is added to the *sNODE* resulting in more accurate predictions (changes are shown in purple.).

modified to accept the augmented input. We leave the output layer of $\hat{\mathbf{f}}_\theta$ unchanged and simply append 1 to the output:

$$\begin{aligned}\hat{\mathbf{f}}_\theta(\hat{\mathbf{x}}_t) &= [\dot{x}_{0_t}, \dot{x}_{1_t}, \dots, \dot{x}_{n-1_t}, \dot{t}]^T \\ &= [\dot{x}_{0_t}, \dot{x}_{1_t}, \dots, \dot{x}_{n-1_t}, 1]^T\end{aligned}\quad (10)$$

This change is done to enable the combination of $\hat{\mathbf{f}}_\theta(\hat{\mathbf{x}}_t)$ with the gradient of the Lyapunov function (in Eq. (4)), which is now defined as

$$\nabla V(\hat{\mathbf{x}}_t) = \left[\frac{\partial V}{\partial x_{0_t}}, \frac{\partial V}{\partial x_{1_t}}, \dots, \frac{\partial V}{\partial x_{n-1_t}}, \frac{\partial V}{\partial t} \right]^T \quad (11)$$

Since the Lyapunov function V_Y produces a scalar value, we only modify the input layer of the ICNN (that models the Lyapunov function) to accept an additional input and leave the output unchanged. In Fig. A.21, we show that this additional time input improves the performance of *s*NODE. We use the *s*NODE model with time input in all our experiments. Also, we use the NODE with time input as a comparative baseline in our experiments since the extra time input has also been shown to be beneficial for the NODE model [7].

B. Learning Position and Orientation Simultaneously

In experiments on the real robot, our models need to learn and predict trajectories of the robot’s position as well as its orientation. Previously [7], this has been achieved by using two separate models (i.e. one model predicts position trajectories, and the other one predicts orientation trajectories). This approach is wasteful because of the number of model parameters is effectively doubled and also because it takes twice as long to train two separate models.

In this paper, we propose an *s*NODE model that can predict position and orientation trajectories simultaneously. As shown in Fig. 3, the human demonstrations that form the training data consist of the position trajectories $\mathbf{p} = \{\mathbf{p}_0, \dots, \mathbf{p}_t, \dots, \mathbf{p}_{T-1}\}$ and orientation trajectories in the

form of quaternion sequences $\mathbf{q} = \{\mathbf{q}_0, \dots, \mathbf{q}_t, \dots, \mathbf{q}_{T-1}\}$, where each $\mathbf{p}_t \in \mathbb{R}^3$ and $\mathbf{q}_t \in \mathbb{S}^3$. The orientation quaternion trajectories are converted to trajectories of rotation vectors $\mathbf{r} = \{\mathbf{r}_0, \dots, \mathbf{r}_t, \dots, \mathbf{r}_{T-1}\}$ (where each $\mathbf{r}_t \in \mathbb{R}^3$) with the help of the *logarithmic map* $\text{Log}(\cdot)$ (see Eq. (5)). The trajectories of these rotation vectors lie in the local Euclidean tangent space. The positions and rotation vectors are combined to form trajectories of 6D vectors $\mathbf{x} = \{\mathbf{x}_0, \dots, \mathbf{x}_t, \dots, \mathbf{x}_{T-1}\}$, where $\mathbf{x}_t = (\mathbf{p}_t, \mathbf{r}_t)$, which are then used to train the *s*NODE model using Eq. (2). For learning real world robot tasks from human demonstrations, we found it useful to scale the rotation vectors using a constant factor before using it for training the model. After training, the *s*NODE predicts trajectories of 6D vectors. The orientation component is converted to the quaternion form with the *exponential map* $\text{Exp}(\cdot)$ (see Eq. (6)).

C. Hypernetwork Models

Hypernetworks have been demonstrated to be the best empirical choice for continual learning from demonstration in [7], where the parameters of a NODE are generated by either a chunked hypernetwork or a regular hypernetwork. In this paper, we propose chunked/regular hypernetwork models that generate the parameters of *two* target networks: (i) a nominal dynamics model that learns and predicts trajectories, and (ii) a parameterized Lyapunov function [6] that enforces stability of the predicted trajectories. This approach leads to improved continual learning performance in addition to convergent, stable trajectory predictions.

Hypernetwork (HN): As shown in Fig. 4 (a), a regular hypernetwork generates the parameters of an *s*NODE $\hat{\mathbf{f}}_\phi$, as defined in Eq. (4), where $\phi = \{\theta, \gamma\}$. Here, θ represents the parameters of the nominal dynamics model \mathbf{f}_θ , and γ represents the parameters of the Lyapunov function V_Y . The parameters ϕ are generated in their entirety from the final layer of the hypernetwork. In the first step of the two-step optimization process, the candidate change $\Delta\mathbf{h}$ of hypernetwork parameters is determined by minimizing the task-specific loss given by Eq. (2):

$$\mathcal{L}^m = \mathcal{L}^m(\phi^m, \mathbf{y}^m) = \frac{1}{2} \sum_t \|\mathbf{y}_t^m - \hat{\mathbf{y}}_t^m\|_2^2 \quad (12)$$

Here, $\phi^m = \{\theta^m, \gamma^m\}$ represents the *s*NODE parameters for the m^{th} task. $\hat{\mathbf{y}}_t^m$ and \mathbf{y}_t^m represent the prediction and ground truth at timestep t for task m respectively. The prediction $\hat{\mathbf{y}}_t^m$ is obtained with Eq. (4). The entire prediction trajectory $\hat{\mathbf{y}}^m$ is obtained by integrating over the t timesteps. In the second optimization step, the hypernetwork parameters and the task embedding vector for task m are optimized as per Eq. (9). In the remainder of this paper, we refer to this model, where an *s*NODE is generated by a regular hypernetwork, as $\text{HN} \rightarrow \text{sNODE}$. In our experiments, we compare against the regular hypernetwork model proposed in [7], and refer to it as $\text{HN} \rightarrow \text{NODE}$.

Chunked Hypernetwork (CHN): As shown in Fig. 4 (b), a chunked hypernetwork generates the parameters $\phi = \{\theta, \gamma\}$ of an *s*NODE $\hat{\mathbf{f}}_\phi$ (Eq. (4)) in segments known as *chunks*. We

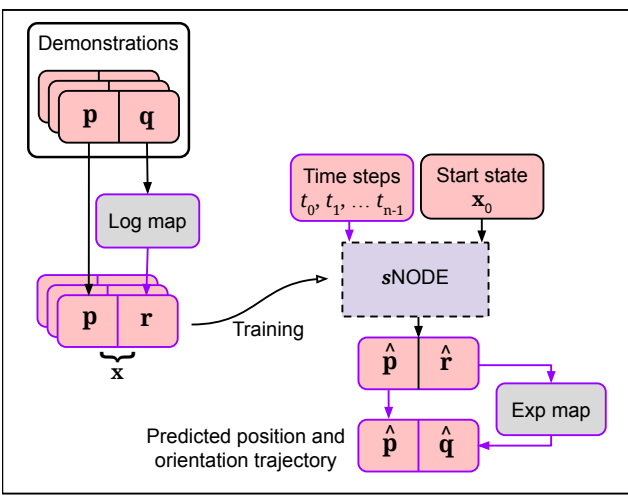


Fig. 3. Trajectories of position and orientation are learned simultaneously by projecting the orientation quaternions into rotation vectors using the Log map, learning trajectories of the positions and rotation vectors in Euclidean space, and then projecting the predicted rotation vectors back into quaternions with the help of the Exp map (for details, see Sec. IV-B).

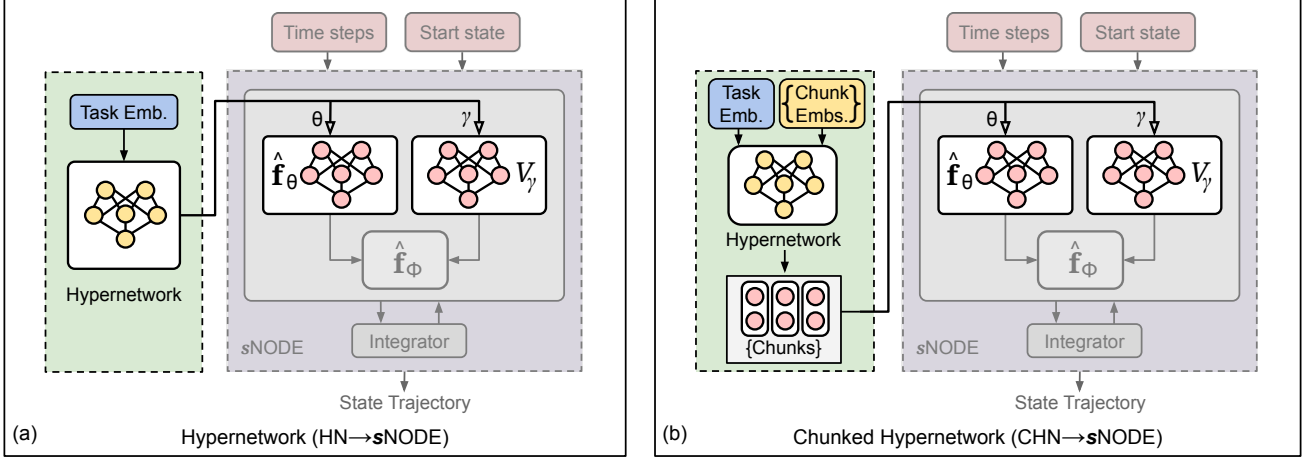


Fig. 4. (a) Architecture of the $\text{HN} \rightarrow \text{sNODE}$ model. Parameters θ and γ of the nominal dynamics model $\hat{\mathbf{f}}_\theta$ and the Lyapunov function V_γ , respectively of the sNODE are generated by the final layer of the Hypernetwork. (b) Architecture of the $\text{CHN} \rightarrow \text{sNODE}$ model. Parameters θ and γ of the sNODE are generated in *chunks* by the Chunked Hypernetwork, allowing for a smaller hypernetwork size. For (a) and (b), the architecture of the sNODE is the same as in Fig. 2 and is shown with muted colors here. Parameters that are learned and are task-specific are shown in █, regularized (task-independent) parameters are shown in █, and non-trainable inputs/outputs are shown in █. Contrary to a stand-alone sNODE , the parameters of the sNODE are not directly trainable, but are simply the outputs of the hypernetworks.

assemble the nominal dynamics model $\hat{\mathbf{f}}_\theta$ and the Lyapunov function V_γ from the generated chunks. Similar to a regular hypernetwork, we use Eq. (12) and Eq. (9) as the two steps of the optimization process for training a chunked hypernetwork. We refer to this model as $\text{CHN} \rightarrow \text{sNODE}$. We treat the $\text{CHN} \rightarrow \text{NODE}$ model from [7] as a comparative baseline, and observe significant improvements in the continual learning performance due to the introduction of sNODE .

D. Stochastic Regularization in Hypernetworks

In spite of demonstrating very good continual learning performance in a variety of domains [7], [10], [33], [42], a shortcoming of hypernetworks is that the regularization effort for training a hypernetwork increases for each new task leading to a cumulative training cost of $\mathcal{O}(N^2)$ for N tasks. This occurs due to the iteration over the stored task embeddings of all previous tasks in Eq. (9). A possible solution to this problem, as proposed in [10], is to use a random subset (of fixed size) of past task embeddings for regularization. Thus, for learning the m^{th} task, the hypernetwork loss function in the second optimization step in Eq. (9) becomes

$$\begin{aligned} \tilde{\mathcal{L}}^m = & \mathcal{L}^m(\theta^m, \mathbf{x}^m) \\ & + \frac{\beta}{|\mathcal{K}|} \sum_{\mathbf{e}^l \in \mathcal{K}}^{\mathcal{K} \sim \text{U}(\mathcal{E}_{m-1})} \|\mathbf{f}(\mathbf{e}^l, \mathbf{h}^*) - \mathbf{f}(\mathbf{e}^l, \mathbf{h} + \Delta \mathbf{h})\|^2 \quad (13) \end{aligned}$$

where \mathcal{K} denotes the random subset of task embeddings sampled uniformly from the set of all past task embeddings $\mathcal{E}_{m-1} = \{\mathbf{e}^0, \dots, \mathbf{e}^{m-1}\}$. Other symbols have the same meaning as in Eq. (9). The size of \mathcal{K} is fixed, and as long as $|\mathcal{K}| \leq m-1$ (i.e. until more tasks than the size of \mathcal{K} have been learned), \mathcal{K} simply includes all past task embeddings. von Oswald et al. [10] show that by setting $|\mathcal{K}| = 32$, a hypernetwork is able to achieve continual learning performance which is only marginally worse than the full regularization for the *Permuted MNIST* continual learning benchmark. This helps

to set an upper bound on the time and effort for hypernetwork training: the cumulative training time increases quadratically till $|\mathcal{K}| \leq m-1$, after which it becomes linear.

Although the continual-LfD scenarios we consider are more challenging than the *Permuted MNIST* benchmark, we show that we can completely remove the summation operation in Eq. (13) without any loss in performance. In each training iteration, we uniformly sample a single past task embedding from the set of all past task embeddings (i.e. $|\mathcal{K}| = 1$) and use this for regularization:

$$\begin{aligned} \tilde{\mathcal{L}}^m = & \mathcal{L}^m(\theta^m, \mathbf{x}^m) + \beta \|\mathbf{f}(\mathbf{e}^k, \mathbf{h}^*) - \mathbf{f}(\mathbf{e}^k, \mathbf{h} + \Delta \mathbf{h})\|^2 \quad (14) \\ \text{where } \mathbf{e}^k \sim & \text{U}(\mathcal{E}_{m-1}) \end{aligned}$$

We demonstrate empirically (see Sec. VI-C and Fig. 19), that for continual learning from demonstration of real-world tasks, the performance of a hypernetwork with our proposed form of stochastic regularization is equivalent to a model where the complete regularization is used. Moreover, with this proposed change, the cumulative training cost of hypernetworks for N tasks becomes $\mathcal{O}(N)$ instead of $\mathcal{O}(N^2)$ (the training time for each new task is approximately constant). This cumulative cost of $\mathcal{O}(N)$ is achieved from the very first task, unlike [10] which requires a burn-in period with quadratic growth.

V. EXPERIMENTAL SETUP

In this section, we describe our experimental setup consisting of the different LfD datasets we evaluate our approach on, the different metrics we report, and the baselines that we compare our approach against. Information about our hardware setup and hyperparameters can be found in the appendix.

A. Datasets

LASA 2D: LASA [11] ($\mathcal{D}_{\text{LASA2D}}$) is a dataset of two dimensional trajectories of different shapes that is widely used in the LfD community [1], [2], [4], [7], [43] to benchmark

model performance. $\mathcal{D}_{\text{LASA2D}}$ contains 30 different tasks, where each task is a collection of 7 similar demonstrations. Each demonstration in each task is a sequence of 1000 2D points. Out of the 30 tasks in $\mathcal{D}_{\text{LASA2D}}$, we use the same 26 tasks that have been used in [7] for evaluation. The other 4 tasks are omitted since they are created by merging together dissimilar trajectories. Fig. 7 shows some examples from $\mathcal{D}_{\text{LASA2D}}$. We chose this dataset since it contains a large number of diverse tasks and is particularly suitable for evaluating the continual learning capability of each model as it strives to learn all 26 tasks of the dataset one by one.

High-dimensional LASA: Although $\mathcal{D}_{\text{LASA2D}}$ provides a long sequence of tasks, all of these tasks involve only 2-dimensional trajectories. To evaluate the scalability of our approach to continual learning of high-dimensional trajectories, and since there is no existing dataset suitable for this purpose, we create high-dimensional analogues of the LASA dataset. We create three datasets $\mathcal{D}_{\text{LASA8D}}$, $\mathcal{D}_{\text{LASA16D}}$, and $\mathcal{D}_{\text{LASA32D}}$ where each dataset contains 10 tasks of 8, 16 and 32 dimensional trajectories respectively. We create these datasets by concatenating multiple tasks chosen uniformly from $\mathcal{D}_{\text{LASA2D}}$ into 1 task. For example, a single task in $\mathcal{D}_{\text{LASA32D}}$ is created by concatenating 16 tasks from $\mathcal{D}_{\text{LASA2D}}$. While concatenating the original tasks from $\mathcal{D}_{\text{LASA2D}}$ to create one task of the high-dimensional datasets, we only use unique tasks. Each high-dimensional dataset is a sequence of 10 tasks $T_{t=0:9}$, where each task contains 7 demonstrations $D_{d=0:6}$ and each demonstration is a sequence of 1000 points $P_{p=0:999}$. The dimension of these points are 8, 16, and 32 for $\mathcal{D}_{\text{LASA8D}}$, $\mathcal{D}_{\text{LASA16D}}$, and $\mathcal{D}_{\text{LASA32D}}$ respectively. Fig. A.28 shows the tasks in $\mathcal{D}_{\text{LASA32D}}$.

RoboTasks9: For evaluation in the real world, we consider tasks in which both the position and orientation of the robot’s end effector vary over time. We add 5 new tasks to the 4 existing tasks of the *RoboTasks* dataset [7], creating a dataset of 9 real-world tasks which we refer to as *RoboTasks9* ($\mathcal{D}_{\text{RoboTasks9}}$). The 9 tasks of $\mathcal{D}_{\text{RoboTasks9}}$ are (i) *box opening*: the lid of a box is opened, (ii) *bottle shelving*: a bottle is placed horizontally on a shelf, (iii) *plate stacking*: a plate is stacked on a table, (iv) *pouring*: coffee beans are poured from a cup into a container, (v) *mat folding*: a mat is folded in half, (vi) *navigating*: an object is carried between obstacles, (vii) *pan on stove*: a pan is transferred from a hanging position to a table, (viii) *scooping*: coffee beans are scooped with a spatula, (ix) *table flipping*: a small table lying on its side is flipped to a standing position. Tasks (v)-(ix) are created by us in this paper. Refer to Fig. 1 (d) for a visual depiction of the 9 tasks of $\mathcal{D}_{\text{RoboTasks9}}$. Each task of $\mathcal{D}_{\text{RoboTasks9}}$ contains 9 demonstrations provided kinsethetically by a human. Each demonstration is a sequence of 1000 steps. In each step of each demonstration, the robot’s position $\mathbf{p} \in \mathbb{R}^3$ and orientation $\mathbf{q} \in \mathbb{S}^3$ are recorded. $\mathcal{D}_{\text{RoboTasks9}}$ allows us to evaluate our approach on tasks that can be expected in the real-world, and the long sequence of 9 tasks is suitable for assessing the continual learning capability of our approach.

B. Metrics

Trajectory Metrics: We measure the accuracy of the predicted trajectories in terms of their similarity to the ground truth demonstrations. For trajectories of the end-effector position, we report the widely-used *Dynamic Time Warping error* (DTW) [2], [7], [44]. For trajectories of the robot’s orientation, we report the commonly used *Quaternion error* [7], [35], [37].

Continual Learning Metrics: To assess the continual learning performance of our models, we report the following 6 metrics which evaluate the models according to a diverse set of criteria: (i) *Accuracy* (ACC) [45]: average accuracy of the trajectories predicted for the current and past tasks, (ii) *Remembering* (REM) [45]: a measure of how well past tasks are remembered, (iii) *Model Size Efficiency* (MS) [45]: how much the size of the model grows compared to its initial size, (iv) *Sample Storage Size Efficiency* (SSS) [45]: how the data storage requirements of a model grows when training data of past tasks is stored, (v) *Time Efficiency* (TE) [7]: increase in training duration with the number of tasks relative to the time taken to learn the first task, and (vi) *Final Model Size* (FS) [7]: A measure of the final parameter size of a model relative to the other models it is compared against. Each of these metrics lies in the range 0 (worst) to 1 (best). Using the set of individual continual learning metrics $\mathcal{C} = \{\text{ACC}, \text{REM}, \text{MS}, \text{SSS}, \text{TE}, \text{FS}\}$, we also report the overall continual learning metrics [45]: $\text{CL}_{\text{score}} = \sum_i^{n(\mathcal{C})} c_i$ and $\text{CL}_{\text{stability}} = 1 - \sum_i^{n(\mathcal{C})} \text{STDEV}(c_i)$

Stability Metrics: We assess the stability (convergence) of the trajectories predicted by our models in two ways. Firstly, we initialize a model at a starting position that is different from the demonstration and then measure the distance between the final point of the predicted trajectory and the goal (final point of the demonstration). For an ideal model, this $\Delta_{\text{goal-position}}$ will be close to zero as the predicted trajectories should converge at the goal. Secondly, we assess whether the trajectories predicted by the model move away from the goal. For this, we make the models predict trajectories of steps greater than those seen in the demonstrations (e.g. demonstrations are of 1000 steps, the model makes predictions for 1100 or 1200 steps). The ideal model’s predicted trajectory in this case should terminate close to the goal irrespective of the number of extra steps.

C. Baselines

Our comparative baselines include continual learning (CL) methods from all families. For each CL method, we consider two versions: one where the task learner is a NODE and another where the task learner is an *s*NODE. We compare our proposed hypernetwork models ($\text{HN} \rightarrow \text{sNODE}$, $\text{CHN} \rightarrow \text{sNODE}$) against $\text{HN} \rightarrow \text{NODE}$, $\text{CHN} \rightarrow \text{NODE}$ and the below baselines:

Single model per task (SG): A single NODE/*s*NODE is used to learn a single task, and is frozen after the task is learned. For predicting the trajectories of the m^{th} task, the m^{th} model is chosen. This setting acts as an upper performance baseline, as the learning of new tasks does not induce forgetting in the previous models.

Finetuning (FT): A single NODE/sNODE is trained on the first task, and then finetuned to learn each subsequent task. This setting acts as the lower performance baseline, since finetuning overwrites the knowledge of past tasks.

Replay (REP): The data of each task is stored and replayed for the training of a NODE/sNODE model on each subsequent task. Following [7], we keep the number of training iterations constant for each task.

Synaptic Intelligence (SI): This setting is similar to FT, but for learning a new task, a regularization loss (Eq. (7)) is used to protect the parameters that are deemed important for remembering past tasks. Refer to [7], [28] for details.

Memory Aware Synapses (MAS): Similar to SI, this is also a direct regularization baseline that uses Eq. (7). The difference is only in the computation of parameter importance. Refer to [7], [29] for further details.

Since during prediction, we need to tell the model which task it should predict trajectories for, the models of FT, REP, SI, and MAS are task-conditioned [7] by an additional input in the form of a task embedding vector.

VI. RESULTS

We present the results of our experiments on the datasets described in Sec. V-A. Experiment hyperparameters and additional results can be found in the appendix.

A. Long Sequence of Tasks: LASA 2D

We consider all the 7 different types of continual learning methods (SG, FT, REP, SI, MAS, HN, CHN) as described in Sec. V, and for each of these CL methods, we consider 2 kinds of task learning approaches: NODE and sNODE. Thus, in total we have 14 different models which we continually train on the 26 tasks of $\mathcal{D}_{\text{LASA2D}}$. After a model has finished learning a task, we evaluate the trajectory errors of the predictions made by the model for the current task as well as all previous tasks. This is repeated for each task, e.g. after learning the m^{th} task in a sequence of T tasks, a model is evaluated on tasks $(0, 1, \dots, m)$. This is repeated for all tasks, i.e. for $m = 0, 1, \dots, T-1$. Each experiment is repeated for 5 independent seeds.

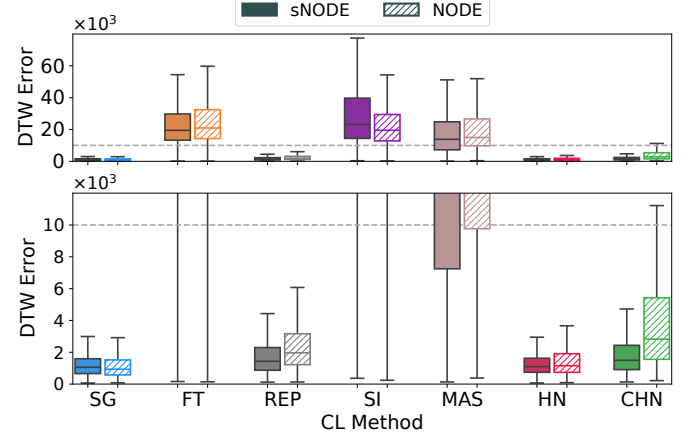


Fig. 6. DTW errors (lower is better) of all predictions while learning the LASA 2D tasks. The bottom row shows a zoomed-in view of the top plot, and the dashed gray line is a reference for comparing the scales of the two plots. Solid boxes depict sNODE and dashed boxes depict NODE. With sNODE as the task learner, HN \blacksquare and CHN \blacksquare outperform regularization based methods (SI \blacksquare , MAS \blacksquare), and perform on par with the upper baselines SG \blacksquare and REP \blacksquare . For SG, there is no perceivable difference between NODE \blacksquare and sNODE \blacksquare , but sNODE improves the continual learning performance of REP (\blacksquare vs \blacksquare), HN (\blacksquare vs \blacksquare) and most considerably that of the smallest model CHN (\blacksquare vs \blacksquare). Results shown are obtained with 5 independent seeds.

We record all the predicted trajectory errors and report the overall errors in Fig. 6 which shows that amongst all the methods, FT, SI, and MAS produce high errors (for both NODE and sNODE), and the hypernetwork methods (HN, CHN) perform on par with the upper baselines SG and REP. The comparison between NODE and sNODE for SG shows that there is no difference in the performance. However, for all the other CL methods that produce low errors (REP, HN, CHN), the errors for sNODE are lower than those for NODE. This difference is the most significant for CHN, the model with the fewest number of parameters.

Fig. 5 shows a more detailed view of the prediction errors after each task is learned during the training process for the CL methods that work the best (SG, REP, HN, and CHN). Here, it can be seen that the CHN \rightarrow sNODE model clearly outperforms the CHN \rightarrow NODE model. With sNODE, the chunked hypernetwork is able to learn and remember all 26

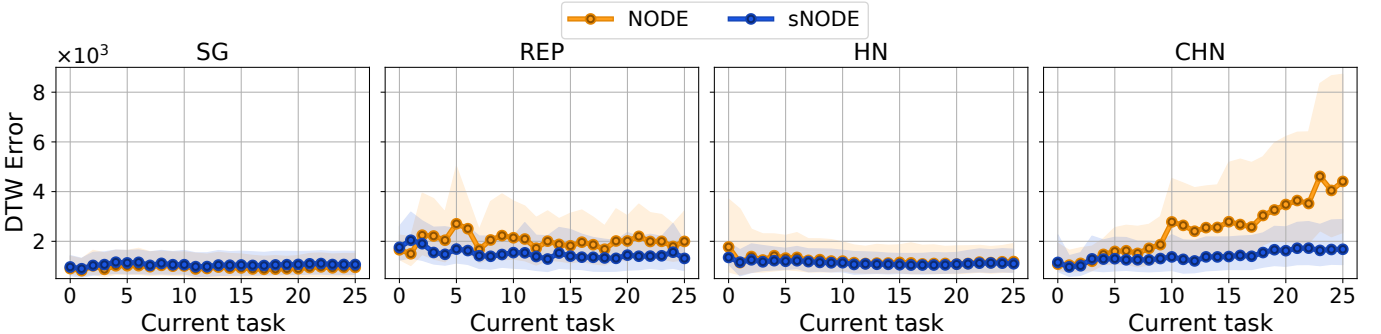


Fig. 5. sNODE improves continual learning performance: DTW errors of trajectories predicted by SG, REP, HN, and CHN while learning the tasks of the LASA dataset (lower is better) are shown. The x-axis shows the current task. After learning each new task, the current and all previous tasks are evaluated. The DTW errors of these predictions are shown on the y-axis. Points show the medians and the shaded region represents the inter-quartile range of results for 5 independent seeds. The performance of SG with NODE and sNODE is equivalent and there are minor improvements for REP and HN with an sNODE. The CHN \rightarrow sNODE model is able to learn and remember all 26 tasks, while the CHN \rightarrow NODE model starts producing high errors after task 5.

tasks of the dataset and its performance is comparable to that of the much larger HN and also to the upper baseline SG. On the other hand, a CHN \rightarrow NODE model can only remember a few tasks and starts to exhibit high errors once the number of tasks exceeds 6. Marginal improvements in performance can also be observed for REP and HN when *s*NODE is used.

Fig. 8 shows that CHN models for both NODE and *s*NODE are the smallest among all the compared models. In spite of having the least number of parameters, the performance of CHN \rightarrow *s*NODE is comparable to that of HN and the upper baseline SG, both of which have many more parameters. The network architectures and exact number of parameters of each model are reported in the appendix.

Next, we report the continual learning metrics that measure the different trade-offs made by the models for learning all the tasks of the LASA dataset. For measuring the continual learning metrics, each prediction has to be classified as either accurate or inaccurate by setting a threshold on the DTW error. For this, we use the same threshold value of 2191 used in [7]. The resulting continual learning metrics for the methods that perform well are reported in Figs. 9 and 10. Complete metrics for all methods are reported in Tab. A.1. Fig. A.22 in the appendix shows a comparison between NODE and *s*NODE models of each method.

Fig. 9 shows that amongst the *s*NODE models that perform well, HN and CHN perform consistently well across all continual learning metrics, unlike SG and REP. Fig. 10 shows

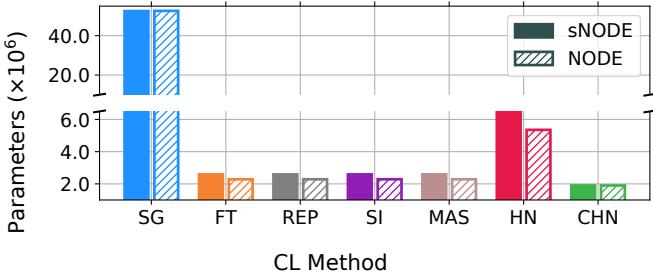


Fig. 8. Parameter counts after learning all 26 tasks of the LASA 2D dataset. We do not show the storage needed by REP to store the data of all tasks. Despite having much fewer parameters than SG and HN, the performance of CHN \rightarrow *s*NODE is equivalent to these larger models.

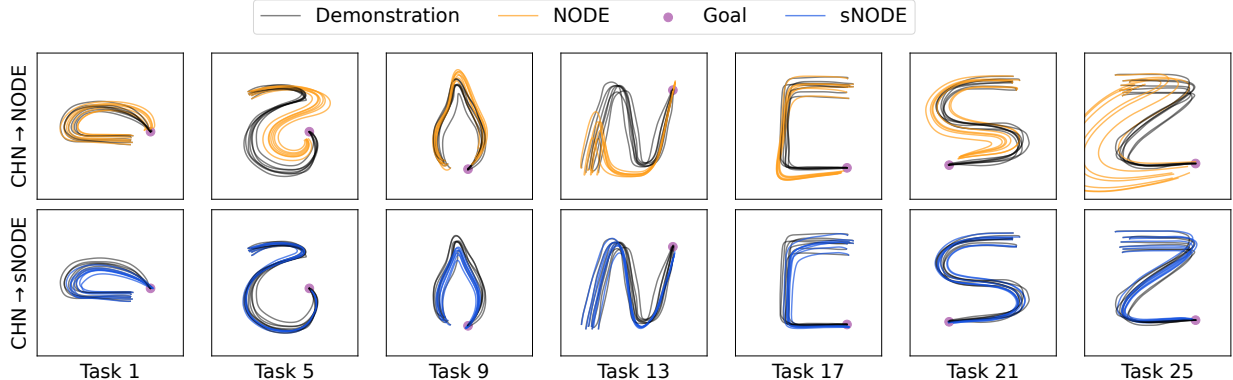


Fig. 7. Qualitative examples of predictions made for the LASA 2D dataset. CHN \rightarrow NODE produces wrong predictions for many tasks, but CHN \rightarrow *s*NODE does not.

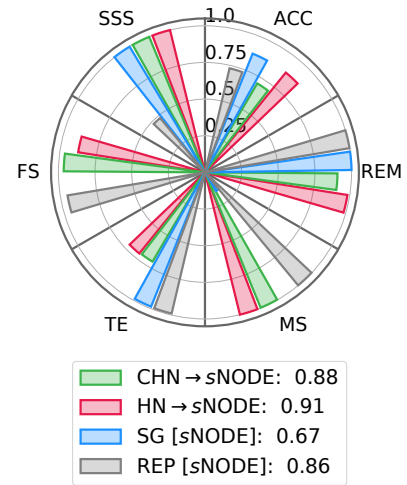


Fig. 9. Continual learning metrics (0:worst-1:best) for SG, REP, HN, and CHN with *s*NODE as the task learner for the LASA 2D dataset. Overall CL score is shown in the legend. SG performs poorly in terms of MS and FS, and REP has a low score in SSS. HN and CHN are the *only* models that perform consistently across all continual learning metrics.

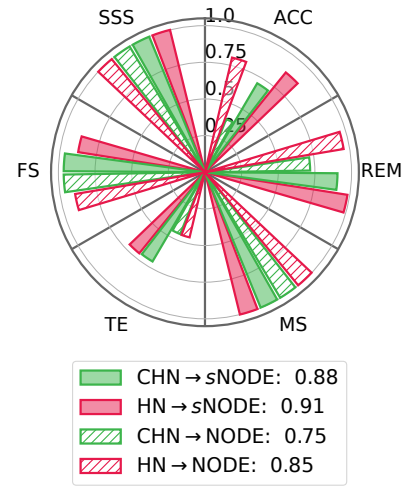


Fig. 10. Continual learning metrics (0:worst-1:best) for CHN \rightarrow NODE, HN \rightarrow NODE, CHN \rightarrow *s*NODE and HN \rightarrow *s*NODE for the LASA 2D dataset. Overall CL score is shown in the legend. CHN \rightarrow *s*NODE outperforms CHN \rightarrow NODE for multiple CL metrics such as ACC, REM and TE.

that $\text{CHN} \rightarrow s\text{NODE}$ outperforms $\text{CHN} \rightarrow \text{NODE}$ in multiple CL metrics. $s\text{NODE}$ also improves the performance of HN and marginally that of REP . In Tab. A.1 it can be observed that amongst all the 14 models, $\text{HN} \rightarrow s\text{NODE}$ and $\text{CHN} \rightarrow s\text{NODE}$ achieve the best overall continual learning score. Fig. 7 shows qualitative results for $\text{CHN} \rightarrow \text{NODE}$ and $\text{CHN} \rightarrow s\text{NODE}$ for $\mathcal{D}_{\text{LASA2D}}$. It can be seen that $\text{CHN} \rightarrow s\text{NODE}$ predicts much more accurate trajectories. In Fig. A.29 and Fig. A.30 in the appendix, we demonstrate that $\text{CHN} \rightarrow s\text{NODE}$ is also much more robust to novel starting configurations than $\text{CHN} \rightarrow \text{NODE}$, which is prone to divergence due to the absence of stability guarantees.

B. High-dimensional Trajectories: LASA 8D, 16D, 32D

The high-dimensional LASA datasets ($\mathcal{D}_{\text{LASA8D}}$, $\mathcal{D}_{\text{LASA16D}}$, $\mathcal{D}_{\text{LASA32D}}$) we create from the original $\mathcal{D}_{\text{LASA2D}}$ dataset represent a more difficult learning challenge that is designed to further test the continual learning capabilities and scalability of our models. For each of these high-dimensional datasets, we repeat the same experiments as for $\mathcal{D}_{\text{LASA2D}}$. We evaluate the CL methods SG, FT, REP, HN, and CHN, and consider two versions of each CL method, corresponding to NODE and $s\text{NODE}$. We omit the direct regularization-based methods SI and MAS due to their poor performance on $\mathcal{D}_{\text{LASA2D}}$, but include FT as a lower performance baseline for reference. All experiments are repeated with 5 independent seeds.

Fig. 12 shows the overall errors for the current and past tasks for all 10 tasks during training for the methods that perform well (FT is excluded in this figure due to its high errors, see Fig. A.23 in the appendix for the complete results including FT). It can be seen that the performance of $\text{HN} \rightarrow \text{NODE}$ is close to that of the upper baseline SG, and $\text{CHN} \rightarrow \text{NODE}$ performs better than REP. Also, $\text{CHN} \rightarrow s\text{NODE}$ performs better than $\text{CHN} \rightarrow \text{NODE}$.

The evaluation errors of the predictions made for the current and past tasks after learning each individual task of $\mathcal{D}_{\text{LASA32D}}$ during training are shown in Fig. 11. Here, we only show the best performing methods, and omit FT due to the much higher scale of its errors. The results for all the high-dimensional datasets ($\mathcal{D}_{\text{LASA8D}}$, $\mathcal{D}_{\text{LASA16D}}$, and $\mathcal{D}_{\text{LASA32D}}$) together can be seen in Fig. A.24 in the appendix. In Fig. 11, it can be seen that $\text{CHN} \rightarrow s\text{NODE}$ produces lower errors compared

to $\text{CHN} \rightarrow \text{NODE}$. This highlights the positive influence that $s\text{NODE}$ has towards improving the performance of CHN. There is negligible difference between NODE and $s\text{NODE}$ for the upper baseline SG and also for HN.

Although the $\text{CHN} \rightarrow s\text{NODE}$ model produces higher errors than SG, after all tasks have been learned, it is still able to predict trajectories for all past tasks using a single model and without revisiting data of past tasks. The predicted trajectories are similar to the ground truth demonstrations, as can be seen from the qualitative examples in Fig. A.28 (in the appendix). Also, note that for each dataset, the size of $\text{CHN} \rightarrow s\text{NODE}$ is

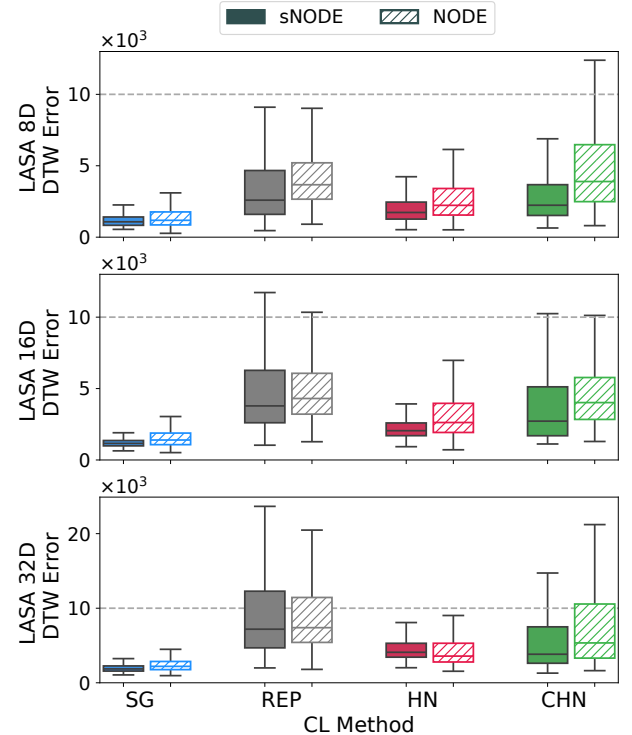


Fig. 12. Comparison of the DTW errors (lower is better) of all predictions while learning the tasks of the high-dimensional LASA datasets. Solid boxes depict $s\text{NODE}$ and dashed boxes depict NODE. The dotted gray line is a reference for comparing the scales of the plots. For SG, there is little difference between NODE and $s\text{NODE}$, but $s\text{NODE}$ improves the continual learning performance of $\text{CHN} \rightarrow s\text{NODE}$ over $\text{CHN} \rightarrow \text{NODE}$, most prominently for LASA 8D and LASA 32D. Results shown are obtained with 5 independent seeds.

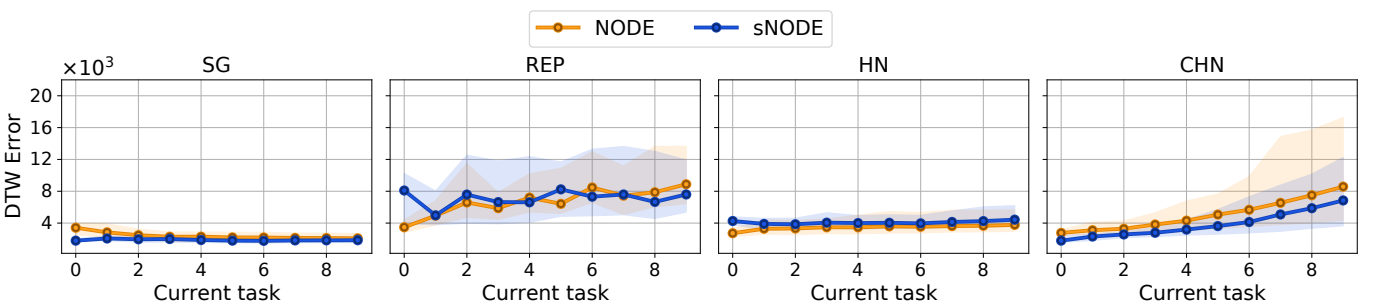


Fig. 11. DTW errors of trajectories predicted by SG, REP, HN, and CHN while learning the tasks of the LASA 32D dataset (lower is better). The x-axis shows the current task. After learning each new task, the current and all previous tasks are evaluated. The DTW errors of these predictions are shown on the y-axis. Lines show the medians and the shaded region represents the inter-quartile range of results for 5 independent seeds. The performances of SG and HN with NODE and $s\text{NODE}$ are equivalent. $\text{CHN} \rightarrow s\text{NODE}$ produces lower median errors than $\text{CHN} \rightarrow \text{NODE}$ and with lower variability in the results.

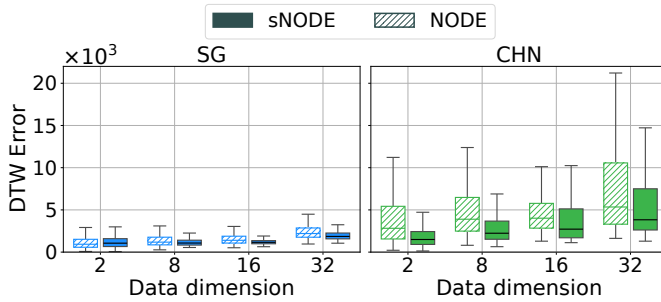


Fig. 14. Comparison of the DTW errors (lower is better) for different dimensions of the trajectories of all the LASA datasets. With an increase in dimensionality, learning becomes more difficult, but CHN \rightarrow sNODE degrades less than CHN \rightarrow NODE.

much smaller than the overall size of the corresponding SG model (refer to Fig. A.27 for the model sizes). This is also reflected in the continual learning metrics of the models for the high-dimensional LASA datasets (Fig. A.26 and Tab. A.3), where the hypernetwork models using sNODE (HN \rightarrow sNODE, CHN \rightarrow sNODE) exhibit the best overall continual learning performance across all the high-dimensional LASA datasets.

With an increase in the trajectory dimension, the difficulty of the continual learning process also increases. To analyze the performance of the CHN models as the trajectory dimension increases, we plot the overall errors for the CHN and SG models for all the LASA datasets (including $\mathcal{D}_{\text{LASA2D}}$) side by side in Fig. 14. Here, it can be seen that for both NODE and sNODE, the errors produced by CHN increase as the trajectory dimension increases from 2 to 32. However, the performance degradation is much more severe for NODE than for sNODE.

C. Real-world Tasks: RoboTasks9

In this paper, we evaluate our approach on the 9 real world tasks of $\mathcal{D}_{\text{RoboTasks9}}$. In each task, trajectories of both the position and orientation of the end-effector of the robot need to be predicted. We evaluate and compare SG, FT, REP, HN and CHN on $\mathcal{D}_{\text{RoboTasks9}}$. In these experiments, 2 versions of each baseline are tested: one where the task learner is a NODE [7], and another where the task learner is an sNODE. As proposed

in Sec. IV-B, our sNODE model can predict positions and orientations together.

We train the 10 different models continually on the 9 tasks of $\mathcal{D}_{\text{RoboTasks9}}$. After each task (in the sequence of 9 tasks) is learned, we evaluate each model on the task it has just learned, as well as on all the previous tasks. In Fig. 13, we compare the overall evaluation errors produced by these models while learning the tasks of $\mathcal{D}_{\text{RoboTasks9}}$. FT is excluded due to its high errors (see Fig. A.32 in the appendix for the full results). It can be seen in Fig. 13 that the position (DTW) and orientation (Quaternion) errors produced by CHN \rightarrow sNODE and HN \rightarrow sNODE are among the lowest and close to those of the upper baseline SG-sNODE (which uses a different model for each task) and REP-sNODE (which reuses the training data from all the past tasks). It can also be observed that sNODE improves the performance of REP, HN and CHN in both the trajectory metrics, while SG with sNODE performs almost equivalently as SG with NODE. Overall, the performance of CHN improves the most when stability is introduced with sNODE.

While Fig. 13 shows the overall prediction errors for each method, in Fig. 15, we show a more granular view of this result to illustrate how the prediction error changes during the sequential training as more tasks are learned. The plots in the top row of Fig. 15 show the position errors, and the bottom row shows the orientation errors for SG, REP, HN, and CHN. These results also confirm that sNODE greatly improves the performance of the continual learning models, particularly REP and CHN. All our experiments are repeated 5 times with independent seeds.

Next, we evaluate the continual learning performance of the different methods on $\mathcal{D}_{\text{RoboTasks9}}$. We set a threshold of 3000 on the DTW position error and a threshold of 0.08 radians (≈ 4.58 degrees) on the orientation error. These thresholds are stricter than the ones used in [7] (where the DTW threshold was 7191 and the orientation error threshold was 10 degrees), and allow us to set a higher bar for evaluating the continual learning performance of the models under consideration. The continual learning metrics for the position predictions of SG, REP, HN and CHN are reported in Figs. 16 and 17. The

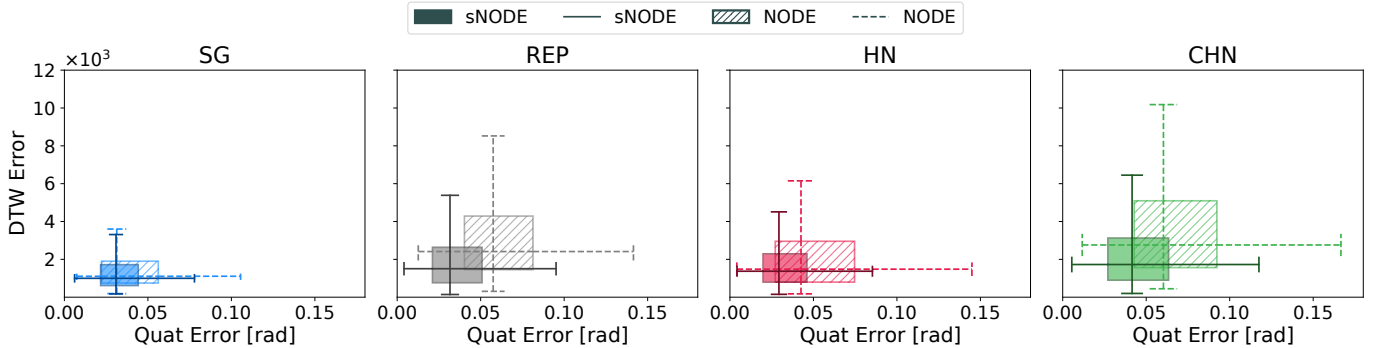


Fig. 13. 2D boxplots showing the position errors (DTW) in the y-axis, and orientation errors (quaternion error) in the x-axis of all predictions while learning the tasks of the RoboTasks9 dataset. Solid boxes depict sNODE and dashed boxes depict NODE. CHN \rightarrow sNODE (green) and HN \rightarrow sNODE (red) are among the best performing methods in spite of using a single model (unlike SG (blue), (blue)) and not retraining on past demonstrations (unlike REP (black), (black)). SG has almost the same performance for sNODE (blue) and NODE (blue) (only minor improvement in quat error). All other methods improve when sNODE is used. CHN \rightarrow sNODE (green) shows the biggest improvement over CHN \rightarrow NODE (green).

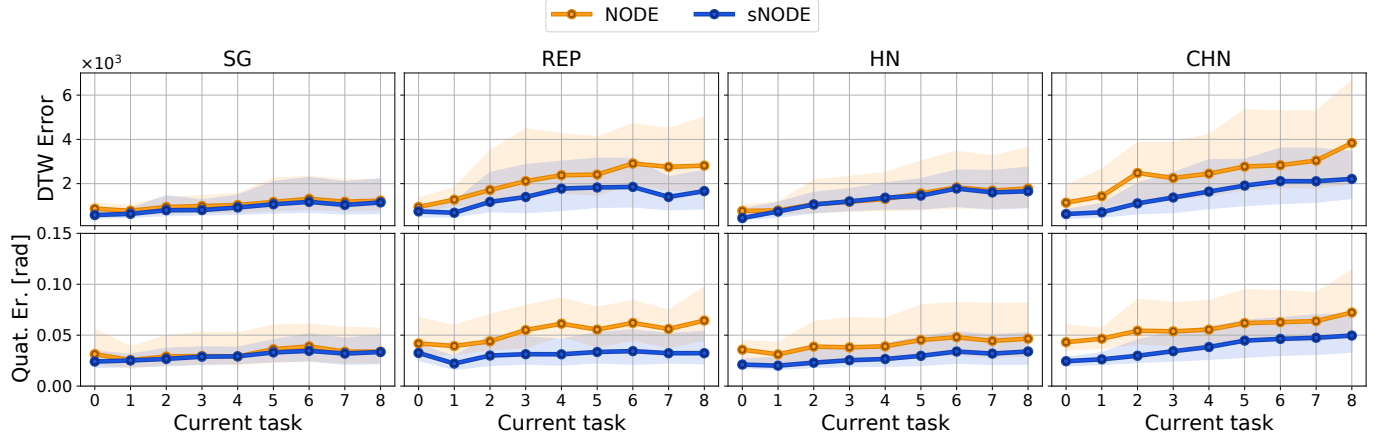


Fig. 15. Position (top) and orientation (bottom) errors of SG, REP, HN, and CHN for the RoboTasks9 dataset (lower is better). The x-axis shows the current task, and the y-axis shows the evaluation errors for the current and all previous tasks. Lines and shaded regions show the medians and inter-quartile ranges respectively for 5 independent seeds. SG with NODE and sNODE is equivalent, but there are improvements for HN and REP with sNODE. CHN \rightarrow sNODE produces lower median errors than CHN \rightarrow NODE and with much less variability in the results.

complete table of CL metrics for both position and orientation for all methods (including FT) are reported in Tab. A.4 and Tab. A.5 respectively (in the appendix). A graphical view of the full results is shown in Fig. A.33. Fig. 16 shows that among the sNODE models, CHN \rightarrow sNODE is the only method with good scores for all CL metrics and thus achieves the highest overall CL score. In Fig. 17, it can be seen that sNODE, both HN and CHN outperform the NODE models, with CHN \rightarrow sNODE exhibiting very good performance in key metrics such as ACC (accuracy) and REM (remembering) that results in the best overall CL score among all methods.

Overall, CHN \rightarrow sNODE offers the best tradeoff for continual learning among the methods we evaluate: its size is relatively small compared to SG (the model sizes are shown in Fig. 18), it can learn and remember multiple tasks without forgetting, it does not need to store and retrain on demonstrations of past tasks (unlike REP), and it predicts stable

trajectories which also helps in improving its performance over CHN \rightarrow NODE. Fig. 20 shows qualitative examples of the predictions for $\mathcal{D}_{\text{RoboTasks9}}$, where it can be seen that CHN \rightarrow sNODE produces much lower errors than CHN \rightarrow NODE.

A limitation of using hypernetworks for continual learning [7], [10] is that the cumulative training time of a hypernetwork increases quadratically with the number of tasks [7], [10]. In this paper, we overcome this limitation by using a form of stochastic hypernetwork regularization in which only a single randomly sampled past task embedding is used for regularization, which leads to a cumulative training time cost of $\mathcal{O}(N)$ for N tasks instead of $\mathcal{O}(N^2)$ (with our approach each new task is learned in roughly the same amount of time). To show this experimentally, we train three different types of CHN \rightarrow sNODE models on $\mathcal{D}_{\text{RoboTasks9}}$ based on the way regularization is performed:

(i) *Full regularization*: A CHN \rightarrow sNODE model is trained

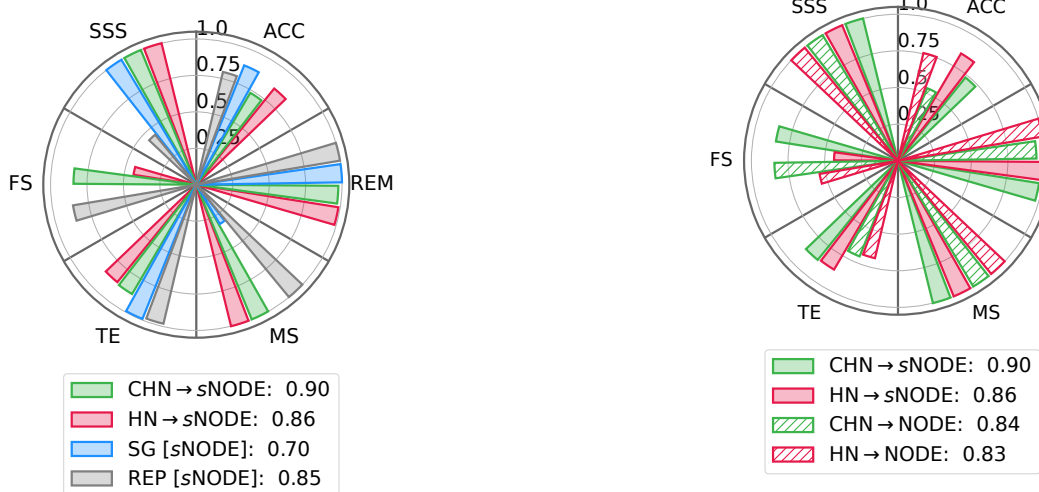


Fig. 16. Continual learning metrics (0:worst-1:best) for SG, REP, HN, and CHN with sNODE as the task learner for the RoboTasks9 dataset. Overall CL scores are shown in the legend. CHN is the only method that performs consistently across all continual learning metrics and has the highest CL score.

Fig. 17. Comparison of continual learning metrics (0:worst-1:best) for HN, and CHN with sNODE and NODE as the task learner for the RoboTasks9 dataset. Overall CL scores are shown in the legend. CHN \rightarrow sNODE is the only method that performs consistently across all continual learning metrics and has the highest CL score.

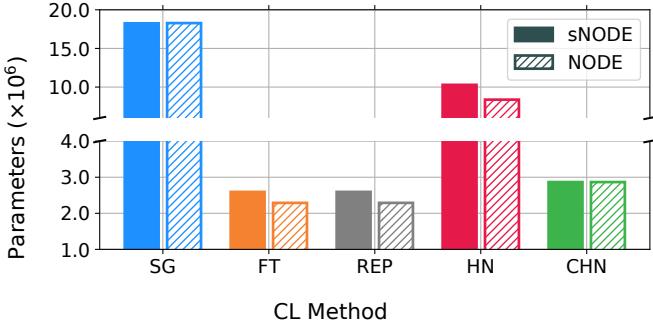


Fig. 18. Parameter counts after learning all 9 tasks of the RoboTasks9 dataset. Even with much fewer parameters than SG and HN, the performance of CHN \rightarrow sNODE is equivalent to these larger models.

using the full hypernetwork regularization in which the task embeddings of all past tasks are used for regularization while learning the current task (as per Eq. (9)). This is the same as the CHN models used in the earlier experiments. We refer to this model as *CHN-all*.

- (ii) *Set-based regularization*: Here, the task embeddings of a fixed number of randomly selected past tasks are considered for regularization while learning the current task (as per Eq. (13)). We consider 2 versions of this model: *CHN-3* and *CHN-5*, which use 3 and 5 randomly selected past task embeddings for regularization respectively.
- (iii) *Single task embedding regularization*: In each iteration during training, a single task embedding is randomly selected from the list of all past task embeddings and is used for regularization (as per Eq. (14)). We refer to this model as *CHN-1*.

We train all 4 models (CHN-all, CHN-5, CHN-3, and CHN-1) on the 9 tasks of $\mathcal{D}_{\text{RoboTasks9}}$, and repeat the experiment 5 times with independent seeds. Similar to before, after each task is learned, we evaluate each model on the current task as well as all the past tasks and repeat this process for all tasks in the sequence. Fig. 19 (top and middle) shows the errors of the trajectory predictions (both positions and orientations) during these evaluations. For reference, we also show the performance of the SG upper baseline in the same plot. In Fig. 19 (bottom), we show the time required for learning each task in the 9-task sequence of $\mathcal{D}_{\text{RoboTasks9}}$.

As can be seen in Fig. 19 (top and middle), the performance of CHN-1 is equivalent to the other CHN models as well as to the upper baseline SG, i.e. performance of a CHN is not impacted by the number of task embeddings used for regularization. However, the use of a single task embedding for regularization enables CHN-1 to achieve $\mathcal{O}(N)$ growth in the cumulative training time for N tasks compared to the $\mathcal{O}(N^2)$ growth for CHN-all, as shown in Fig. 19 (bottom). CHN-3 and CHN-5 also have $\mathcal{O}(N^2)$ growth till 3 and 5 tasks respectively are learned. The performance of SG is marginally better than that for CHN-1, but note that SG uses a separate model for each task resulting in a much larger overall parameter size (as shown in Fig. 18) and much worse overall continual learning performance (as shown in Fig. 16).

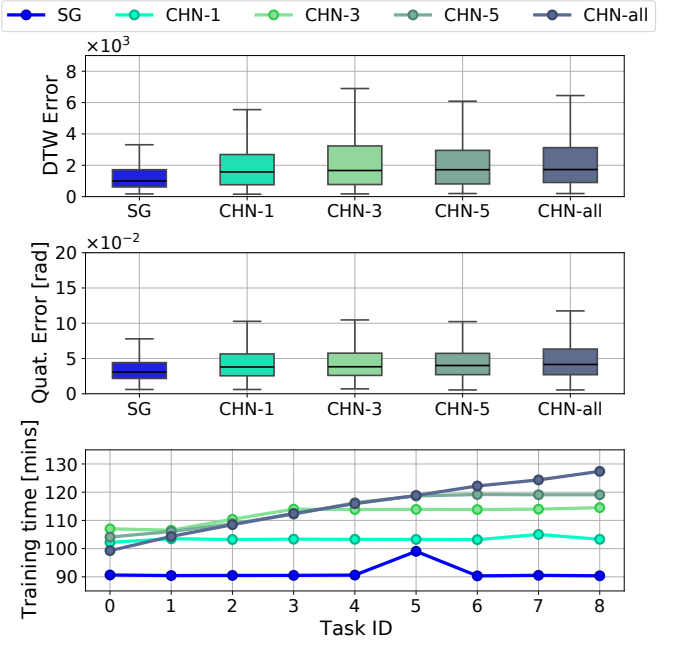


Fig. 19. Stochastic regularization in CHN \rightarrow sNODE for the RoboTasks9 dataset: (top) position errors, (middle) orientation errors, and (bottom) training time for each task. The upper baseline SG (using sNODE) provides the reference for good performance, but has many more parameters than the CHN models. CHN-1 (ours), CHN-3, and CHN-5 use 1, 3 and 5 randomly selected task embeddings for regularization respectively. CHN-all uses all available task embeddings. CHN-1 performs equivalently to the other models, but its training time for each new task stays roughly the same, leading to cumulative training cost of $\mathcal{O}(N)$ for N tasks. The cumulative cost for CHN-3, and CHN-5 increases quadratically till 3 and 5 tasks are learned respectively. CHN-all has a cumulative cost of $\mathcal{O}(N^2)$ for N tasks.

VII. DISCUSSION

Across all the datasets ($\mathcal{D}_{\text{LASA2D}}$, $\mathcal{D}_{\text{LASA8D}}$, $\mathcal{D}_{\text{LASA16D}}$, $\mathcal{D}_{\text{LASA32D}}$, $\mathcal{D}_{\text{RoboTasks9}}$) we evaluate, hypernetwork models emerge as the most promising choice empirically for continual-LfD. Factors such as minimal parameter growth with new tasks, the ability to only use the current data for learning, and their overall continual learning performance make them a robust option for continual LfD. Moreover, we demonstrated that stability within the task learner not only yields more accurate trajectory predictions but also significantly enhances the overall continual learning performance of hypernetworks. This effect is particularly pronounced in the case of smaller chunked hypernetworks. It appears that the constraints imposed by stability requirements compel the model to make more efficient use of its limited set of parameters, leading to improved results.

Our proposed CHN \rightarrow sNODE model successfully learns long sequences of tasks, encompassing high-dimensional trajectories of up to 32 dimensions, as well as real-world robotic LfD tasks with a relatively small set of learnable parameters. This positions CHN \rightarrow sNODE as a viable option for continual learning on resource-constrained robotic platforms. Additionally, the introduction of stochastic regularization with a single task embedding substantially reduces the time required for training while maintaining overall performance, thereby making hypernetworks suitable for real-world applications.

In the future, our work may extend towards devising methods to effectively chain together multiple tasks learned by a CHN/HN model, or perhaps to develop a high-level planner that leverages the diverse set of learned tasks as a versatile skill library for more complex applications.

VIII. CONCLUSION

In this paper, we presented an approach for continual learning from demonstration with hypernetwork-generated stable dynamics models. By evaluating our models on 5 different datasets, we demonstrated empirically that the stability guarantees provided by *s*NODE regarding the predicted trajectories not only result in convergent trajectories, but also improve the continual learning performance and scalability of

our hypernetwork models to high-dimensional trajectories as well as to real-world tasks. These benefits are most pronounced in the size-efficient chunked hypernetworks that achieve the highest overall continual learning score when multiple factors such as accuracy, remembering ability and parameter size are taken into account. Additionally, we also demonstrated the effectiveness of stochastic hypernetwork regularization with a single task embedding that enables hypernetworks to scale efficiently to long task sequences.

REFERENCES

[1] H. Ravichandar, A. S. Polydoros, S. Chernova, and A. Billard, “Recent advances in robot learning from demonstration,” *Annual review of control, robotics, and autonomous systems*, vol. 3, pp. 297–330, 2020.

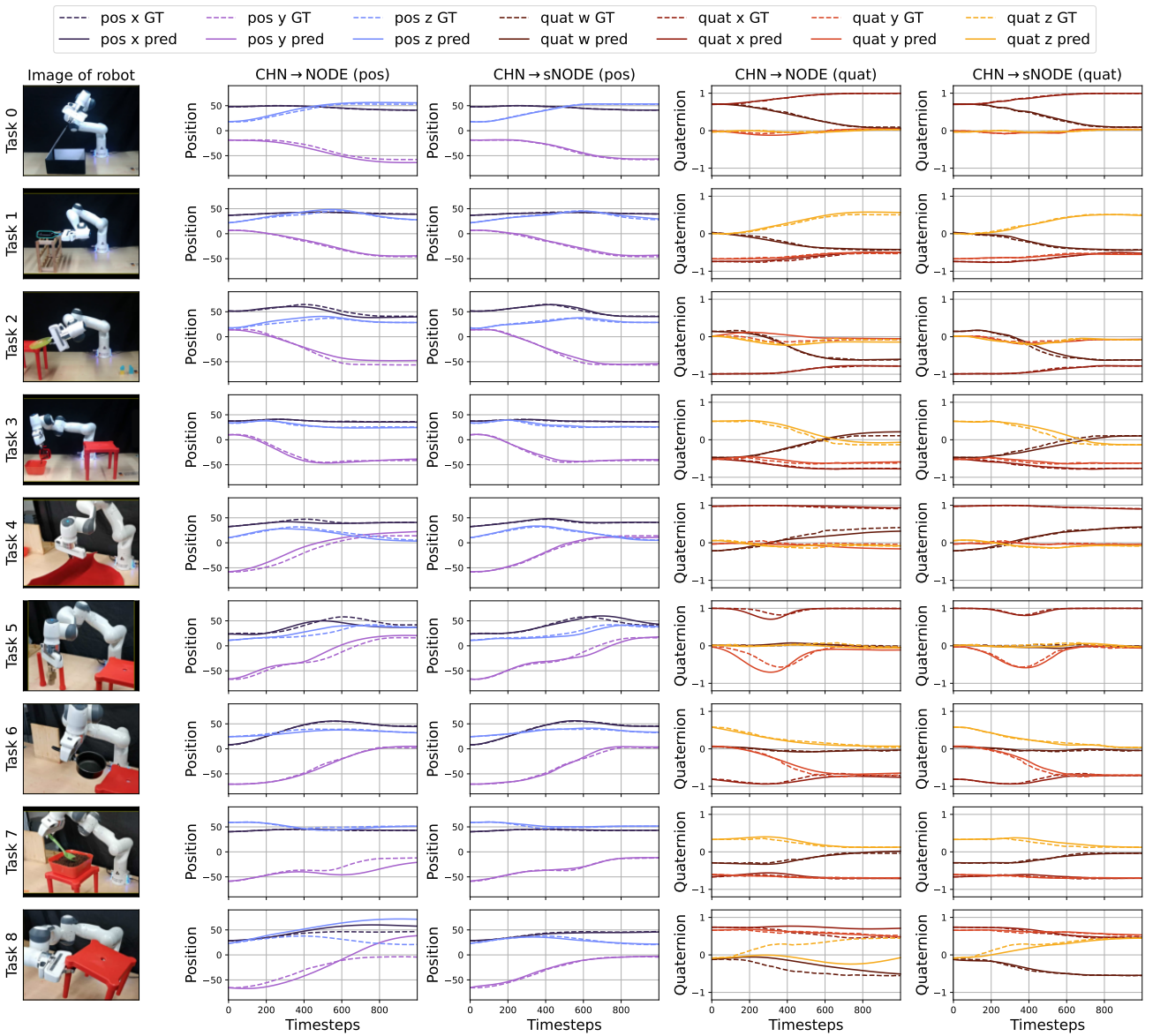


Fig. 20. Qualitative examples for the RoboTasks dataset. Models of CHN→NODE and CHN→*s*NODE are trained sequentially on the 9 tasks of the dataset, and after the last task has been learned, each model is made to perform all the previous tasks. The first column shows images of the robot controlled by CHN→*s*NODE. The second and third columns show the positions predicted by CHN→NODE and CHN→*s*NODE respectively. The fourth and fifth columns show the quaternions predicted by CHN→NODE and CHN→*s*NODE respectively. In the line plots, dotted lines denote the ground truth demonstration and solid lines indicate the predictions. Each row shows a different task. Note the larger errors produced by CHN→NODE compared to CHN→*s*NODE, particularly for tasks 8, 7, 5, and 4.

[2] J. Uraín, M. Ginesi, D. Tateo, and J. Peters, "Imitationflow: Learning deep stable stochastic dynamic systems by normalizing flows," in *2020 IEEE/RSJ International Conference on Intelligent Robots and Systems (IROS)*. IEEE, 2020, pp. 5231–5237.

[3] M. Hersch, F. Guenter, S. Calinon, and A. Billard, "Dynamical system modulation for robot learning via kinesthetic demonstrations," *IEEE Transactions on Robotics*, vol. 24, no. 6, pp. 1463–1467, 2008.

[4] M. Saveriano, "An energy-based approach to ensure the stability of learned dynamical systems," in *IEEE International Conference on Robotics and Automation (ICRA)*, 2020, pp. 4407–4413.

[5] S. M. Khansari-Zadeh and A. Billard, "Learning control lyapunov function to ensure stability of dynamical system-based robot reaching motions," *Robotics and Autonomous Systems*, vol. 62, no. 6, pp. 752–765, 2014.

[6] J. Z. Kolter and G. Manek, "Learning stable deep dynamics models," *Advances in Neural Information Processing Systems*, vol. 32, pp. 11 128–11 136, 2019.

[7] S. Audy, J. Hollenstein, M. Saveriano, A. Rodriguez-Sánchez, and J. Piater, "Continual learning from demonstration of robotics skills," *Robotics and Autonomous Systems*, vol. 165, p. 104427, 2023. [Online]. Available: <https://www.sciencedirect.com/science/article/pii/S0921889023000660>

[8] R. T. Chen, Y. Rubanova, J. Bettencourt, and D. Duvenaud, "Neural ordinary differential equations," in *Proceedings of the 32nd International Conference on Neural Information Processing Systems*, 2018, pp. 6572–6583.

[9] D. Ha, A. M. Dai, and Q. V. Le, "Hypernetworks," in *International Conference on Learning Representations*, 2017. [Online]. Available: <https://openreview.net/forum?id=rkpACe1lx>

[10] J. von Oswald, C. Henning, J. Sacramento, and B. F. Grawe, "Continual learning with hypernetworks," in *International Conference on Learning Representations (ICLR)*, 2019.

[11] S. M. Khansari-Zadeh and A. Billard, "Learning stable nonlinear dynamical systems with Gaussian mixture models," *IEEE Transactions on Robotics*, vol. 27, no. 5, pp. 943–957, 2011.

[12] G. I. Parisi, R. Kemker, J. L. Part, C. Kanan, and S. Wermter, "Continual lifelong learning with neural networks: A review," *Neural Networks*, vol. 113, pp. 54–71, 2019.

[13] A. Billard, S. Calinon, and R. Dillmann, "Learning from humans," *Springer Handbook of Robotics*, 2nd Ed., 2016.

[14] S. Calinon, "Learning from demonstration (programming by demonstration)," *Encyclopedia of robotics*, pp. 1–8, 2018.

[15] B. D. Argall, S. Chernova, M. Veloso, and B. Browning, "A survey of robot learning from demonstration," *Robotics and autonomous systems*, vol. 57, no. 5, pp. 469–483, 2009.

[16] H. Ravichandar, A. Polydoros, S. Chernova, and A. Billard, "Robot learning from demonstration: A review of recent advances," *Annual Review of Control, Robotics, and Autonomous Systems*, 2019.

[17] S. R. Ahmadzadeh and S. Chernova, "Trajectory-based skill learning using generalized cylinders," *Frontiers in Robotics and AI*, vol. 5, p. 132, 2018.

[18] Y. Wu and Y. Demiris, "Towards one shot learning by imitation for humanoid robots," in *2010 IEEE international conference on robotics and automation*. IEEE, 2010, pp. 2889–2894.

[19] B. D. Argall, B. Browning, and M. M. Veloso, "Teacher feedback to scaffold and refine demonstrated motion primitives on a mobile robot," *Robotics and Autonomous Systems*, vol. 59, no. 3-4, pp. 243–255, 2011.

[20] S. Calinon, P. Kormushev, and D. G. Caldwell, "Compliant skills acquisition and multi-optima policy search with em-based reinforcement learning," *Robotics and Autonomous Systems*, vol. 61, no. 4, pp. 369–379, 2013.

[21] N. Das, S. Bechtle, T. Davchev, D. Jayaraman, A. Rai, and F. Meier, "Model-based inverse reinforcement learning from visual demonstrations," in *Conference on Robot Learning*. PMLR, 2021, pp. 1930–1942.

[22] P. Englert, N. A. Vien, and M. Toussaint, "Inverse kkt: Learning cost functions of manipulation tasks from demonstrations," *The International Journal of Robotics Research*, vol. 36, no. 13-14, pp. 1474–1488, 2017.

[23] A. Kalinowska, A. Prabhakar, K. Fitzsimons, and T. Murphrey, "Ergodic imitation: Learning from what to do and what not to do," in *2021 IEEE International Conference on Robotics and Automation (ICRA)*. IEEE, 2021, pp. 3648–3654.

[24] A. J. Ijspeert, J. Nakanishi, and S. Schaal, "Movement imitation with nonlinear dynamical systems in humanoid robots," in *International Conference on Robotics and Automation (ICRA)*, 2002, pp. 1398–1403.

[25] A. A. Rusu, N. C. Rabinowitz, G. Desjardins, H. Soyer, J. Kirkpatrick, K. Kavukcuoglu, R. Pascanu, and R. Hadsell, "Progressive neural networks," *arXiv preprint arXiv:1606.04671*, 2016.

[26] S.-A. Rebiffé, A. Kolesnikov, G. Sperl, and C. H. Lampert, "icarl: Incremental classifier and representation learning," in *Proceedings of the IEEE Conference on Computer Vision and Pattern Recognition*, 2017, pp. 2001–2010.

[27] H. Shin, J. K. Lee, J. Kim, and J. Kim, "Continual learning with deep generative replay," in *Proceedings of the 31st International Conference on Neural Information Processing Systems*, 2017, pp. 2994–3003.

[28] F. Zenke, B. Poole, and S. Ganguli, "Continual learning through synaptic intelligence," in *International Conference on Machine Learning*. PMLR, 2017, pp. 3987–3995.

[29] R. Aljundi, F. Babiloni, M. Elhoseiny, M. Rohrbach, and T. Tuytelaars, "Memory aware synapses: Learning what (not) to forget," in *Proceedings of the European Conference on Computer Vision (ECCV)*, 2018, pp. 139–154.

[30] M. Delange, R. Aljundi, M. Masana, S. Parisot, X. Jia, A. Leonardis, G. Slabaugh, and T. Tuytelaars, "A continual learning survey: Defying forgetting in classification tasks," *IEEE Transactions on Pattern Analysis and Machine Intelligence*, 2021.

[31] C. Gao, H. Gao, S. Guo, T. Zhang, and F. Chen, "CRIL: Continual robot imitation learning via generative and prediction model," in *2021 IEEE/RSJ International Conference on Intelligent Robots and Systems (IROS)*, 2021, pp. 6747–6754.

[32] A. Xie and C. Finn, "Lifelong robotic reinforcement learning by retaining experiences," *arXiv preprint arXiv:2109.09180*, 2021.

[33] Y. Huang, K. Xie, H. Bharadhwaj, and F. Shkurti, "Continual model-based reinforcement learning with hypernetworks," in *2021 IEEE International Conference on Robotics and Automation (ICRA)*. IEEE, 2021, pp. 799–805.

[34] B. Amos, L. Xu, and J. Z. Kolter, "Input convex neural networks," in *International Conference on Machine Learning*. PMLR, 2017, pp. 146–155.

[35] A. Ude, B. Nemeć, T. Petrić, and J. Morimoto, "Orientation in cartesian space dynamic movement primitives," in *2014 IEEE International Conference on Robotics and Automation (ICRA)*. IEEE, 2014, pp. 2997–3004.

[36] Y. Huang, F. J. Abu-Dakka, J. Silvério, and D. G. Caldwell, "Toward orientation learning and adaptation in cartesian space," *IEEE Transactions on Robotics*, vol. 37, no. 1, pp. 82–98, 2020.

[37] M. Saveriano, F. Franzel, and D. Lee, "Merging position and orientation motion primitives," in *2019 International Conference on Robotics and Automation (ICRA)*. IEEE, 2019, pp. 7041–7047.

[38] X. Li, Y. Zhou, T. Wu, R. Socher, and C. Xiong, "Learn to grow: A continual structure learning framework for overcoming catastrophic forgetting," in *International Conference on Machine Learning*. PMLR, 2019, pp. 3925–3934.

[39] J. Yoon, E. Yang, J. Lee, and S. J. Hwang, "Lifelong learning with dynamically expandable networks," in *International Conference on Learning Representations*.

[40] J. Kirkpatrick, R. Pascanu, N. Rabinowitz, J. Veness, G. Desjardins, A. A. Rusu, K. Milan, J. Quan, T. Ramalho, A. Grabska-Barwinska *et al.*, "Overcoming catastrophic forgetting in neural networks," *Proceedings of the national academy of sciences*, vol. 114, no. 13, pp. 3521–3526, 2017.

[41] J. M. Lee, "Introduction to smooth manifolds," 2003.

[42] D. Brahma, V. K. Verma, and P. Rai, "Hypernetworks for continual semi-supervised learning," *arXiv preprint arXiv:2110.01856*, 2021.

[43] C. Blocher, M. Saveriano, and D. Lee, "Learning stable dynamical systems using contraction theory," in *2017 14th International Conference on Ubiquitous Robots and Ambient Intelligence (URAI)*. IEEE, 2017, pp. 124–129.

[44] C. F. Jekel, G. Venter, M. P. Venter, N. Stander, and R. T. Haftka, "Similarity measures for identifying material parameters from hysteresis loops using inverse analysis," *International Journal of Material Forming*, vol. 12, no. 3, pp. 355–378, 2019.

[45] N. Díaz-Rodríguez, V. Lomonaco, D. Filliat, and D. Maltoni, "Don't forget, there is more than forgetting: new metrics for continual learning," *arXiv preprint arXiv:1810.13166*, 2018.

APPENDIX

We present the benefit of introducing the additional time input to the *s*NODE model, as described in Sec. IV-A. For this, we train a separate *s*NODE model on each of the 26 tasks of $\mathcal{D}_{\text{LASA2D}}$. We train two versions of the *s*NODE model: the original model proposed by [6], which is independent of the time input (we refer to this as *s*NODE-I), and an *s*NODE model with our modification of adding the time input (we refer to this as *s*NODE-T). After learning a task, each model is evaluated on the task it has learned. Each experiment is repeated 5 times with independent seeds. As can be seen in Fig. A.21, *s*NODE-T produces lower median DTW errors and a smaller variance in performance for all 26 tasks. Accordingly, in this paper, we use *s*NODE-T in all our experiments and we refer to it simply as *s*NODE. Also, in all experiments, we use the NODE model with time input (NODE-T). For this too, we omit the -T ending for brevity.

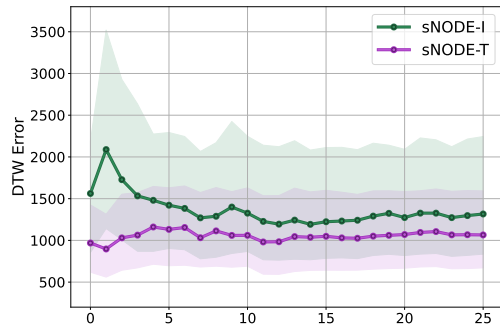


Fig. A.21. Comparison of position errors of predictions (lower is better) produced by *s*NODE with time input (*s*NODE-T) (ours), and the original *s*NODE model without any time input (*s*NODE-I) on the 26 tasks of $\mathcal{D}_{\text{LASA2D}}$. *s*NODE-T produces lower errors and less variability than *s*NODE-I for all tasks.

MET	ACC	REM	MS	TE	FS	SSS	CL _{sco}	CL _{stab}
SG	0.89	1.00	0.15	0.99	0.00	1.00	0.67	0.53
FT	0.06	0.19	1.00	0.99	0.96	1.00	0.70	0.55
REP	0.56	1.00	1.00	0.99	0.96	0.48	0.83	0.76
SI	0.05	0.36	1.00	0.92	0.78	1.00	0.68	0.61
MAS	0.01	0.87	1.00	0.89	0.83	1.00	0.76	0.62
HN	0.80	0.96	1.00	0.46	0.90	1.00	0.85	0.79
CHN	0.39	0.72	1.00	0.45	0.96	1.00	0.75	0.72

(a) NODE

MET	ACC	REM	MS	TE	FS	SSS	CL _{sco}	CL _{stab}
SG	0.87	1.00	0.15	0.99	0.00	1.00	0.67	0.54
FT	0.06	0.20	1.00	0.98	0.95	1.00	0.70	0.56
REP	0.73	1.00	1.00	0.99	0.95	0.48	0.86	0.79
SI	0.02	0.53	1.00	0.97	0.75	1.00	0.71	0.62
MAS	0.08	0.38	1.00	0.86	0.80	1.00	0.69	0.63
HN	0.88	0.98	1.00	0.71	0.88	1.00	0.91	0.89
CHN	0.70	0.90	1.00	0.71	0.96	1.00	0.88	0.86

(b) *s*NODE

TABLE A.1

CONTINUAL LEARNING METRICS FOR THE LASA 2D DATASET (MEDIAN OVER 5 SEEDS). VALUES RANGE FROM 0 (WORST) TO 1 (BEST).
 HN → *s*NODE, FOLLOWED BY CHN → NODE ACHIEVE THE BEST OVERALL CONTINUAL LEARNING SCORE AMONGST ALL METHODS.

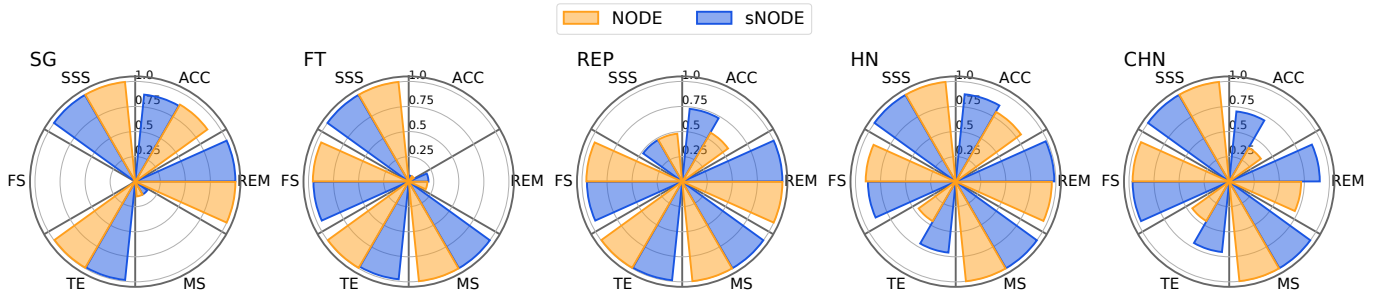


Fig. A.22. *sNODE* improves continual learning for REP, HN and particularly for CHN: Continual learning metrics (0:worst-1:best) for SG, FT, REP, HN, and CHN for the LASA 2D dataset are shown. The scores for both task learners (NODE and *sNODE*) are shown.

Dataset	LASA 2D	LASA 8D	LASA 16D	LASA 32D	RoboTasks9
Dimension	2	8	16	32	6
Iterations	1.5×10^4	6.0×10^4	7.0×10^4	8.0×10^4	4.0×10^4
LR	1.0×10^{-4}	5.0×10^{-5}	5.0×10^{-5}	5.0×10^{-5}	5.0×10^{-5}
SI C	0.3	-	-	-	-
SI ϵ	0.3	-	-	-	-
MAS λ	0.1	-	-	-	-
arch(NODE)	[1000]x2, 1015	[1000]x3, 1015	[1000]x4, 1015	[1000]x5, 1015	[1000]x2, 1015
arch(<i>sNODE</i> \hat{f})	[1000]x3	[1000]x3	[1000]x3	[1000]x3	[1000]x3
arch(<i>sNODE</i> V)	[100]x2	[100]x2	[100]x2	[100]x2	[100]x2
arch(HN NODE)	[100]x2, 150	[100]x3, 150	[100]x4, 150	[80]x5, 100	[100]x2, 150
arch(HN <i>sNODE</i> \hat{f})	[100]x3	[90]x3	[75]x3	[60]x3	[100]x3
arch(HN/CHN)	[200]x3	[300]x3	[300]x3	[350]x3	[300]x3
dim(Task Emb)	256	256	256	512	256
HN/CHN β	5.0×10^{-3}				
dim(CHN Chunk Emb)	256	256	256	512	256
dim(CHN Chunk)	8192	16384	16384	16384	8192
Tangent vector scale	-	-	-	-	5.0

TABLE A.2

HYPERPARAMETERS USED IN OUR EXPERIMENTS. THE SAME NODE AND *sNODE* ARCHITECTURES ARE USED FOR SG, REP, FT, SI, MAS AND CHN. SMALLER NETWORKS FOR NODE AND *sNODE* ARE USED FOR HN TO KEEP THE HYPERNETWORK SIZE COMPARABLE. TANGENT VECTOR SCALE IS USED ONLY WHEN ORIENTATIONS ARE LEARNED FOR THE ROBOTASKS9 DATASET.

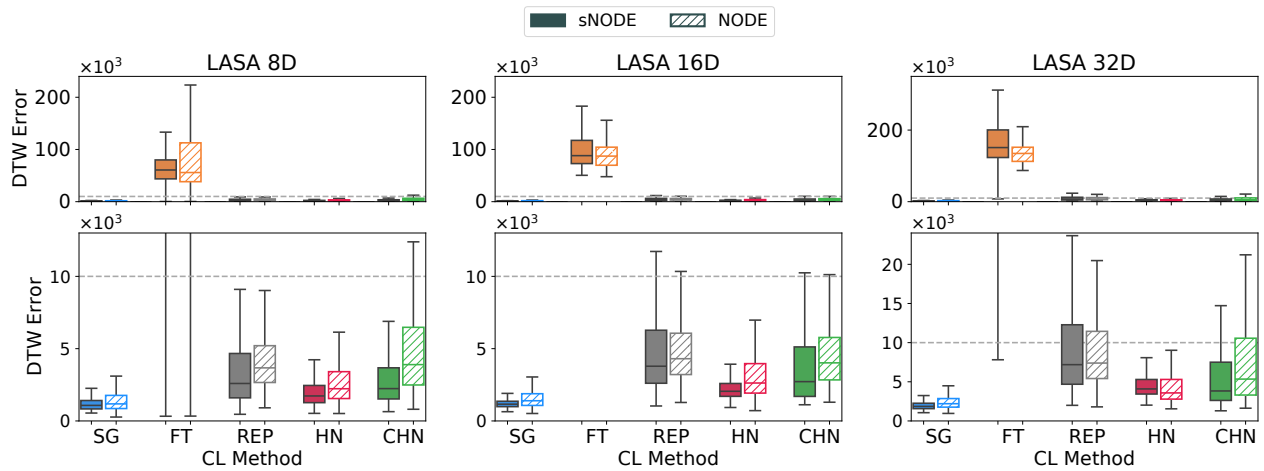


Fig. A.23. Comparison of the DTW errors (lower is better) of all predictions while learning the the tasks of the high-dimensional LASA datasets. The bottom row shows a zoomed-in view. The dotted gray line is a reference for comparing the scales of the top and bottom plots. For SG, there is there is very little difference between NODE and *sNODE*, but *sNODE* improves the continual learning performance of HN and CHN. The improvement is the most considerable for CHN \rightarrow *sNODE*. Results shown are obtained with 5 independent seeds.

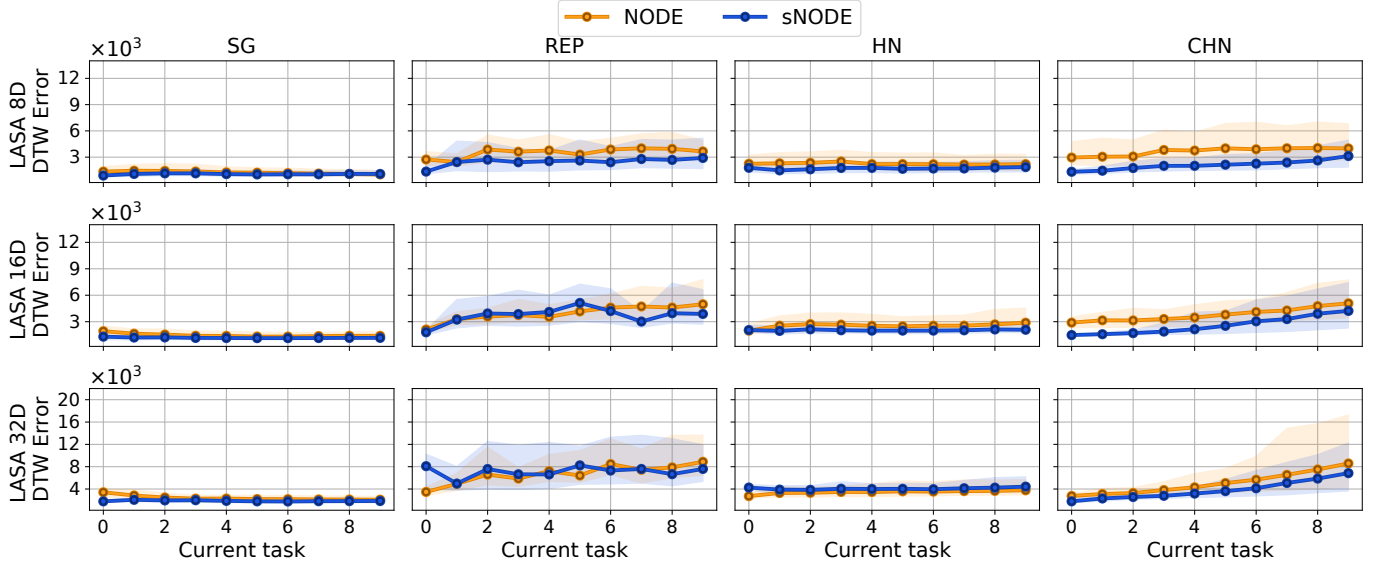


Fig. A.24. DTW errors of trajectories predicted by SG, REP, HN, and CHN while learning the tasks of the LASA dataset (lower is better). The x-axis shows the current task. After learning each new task, the current and all previous tasks are evaluated. The DTW errors of these predictions are shown on the y-axis. Lines show the medians and the shaded region represents the inter-quartile range of results for 5 independent seeds. The performance of SG with NODE and sNODE is equivalent and there are minor improvements for HN with an sNODE. CHN→sNODE is able to remember all tasks and produces lower median errors than CHN→NODE and with lower variability in the results.

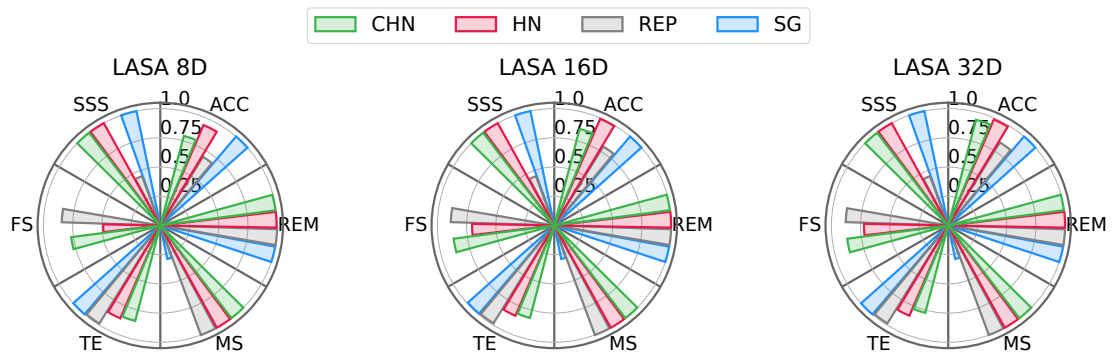


Fig. A.25. Continual learning metrics (0:worst-1:best) for SG, REP, HN, and CHN with sNODE as the task learner for the high-dimensional LASA datasets. CHN performs consistently across all continual learning metrics. Results shown are obtained using 5 independent seeds.

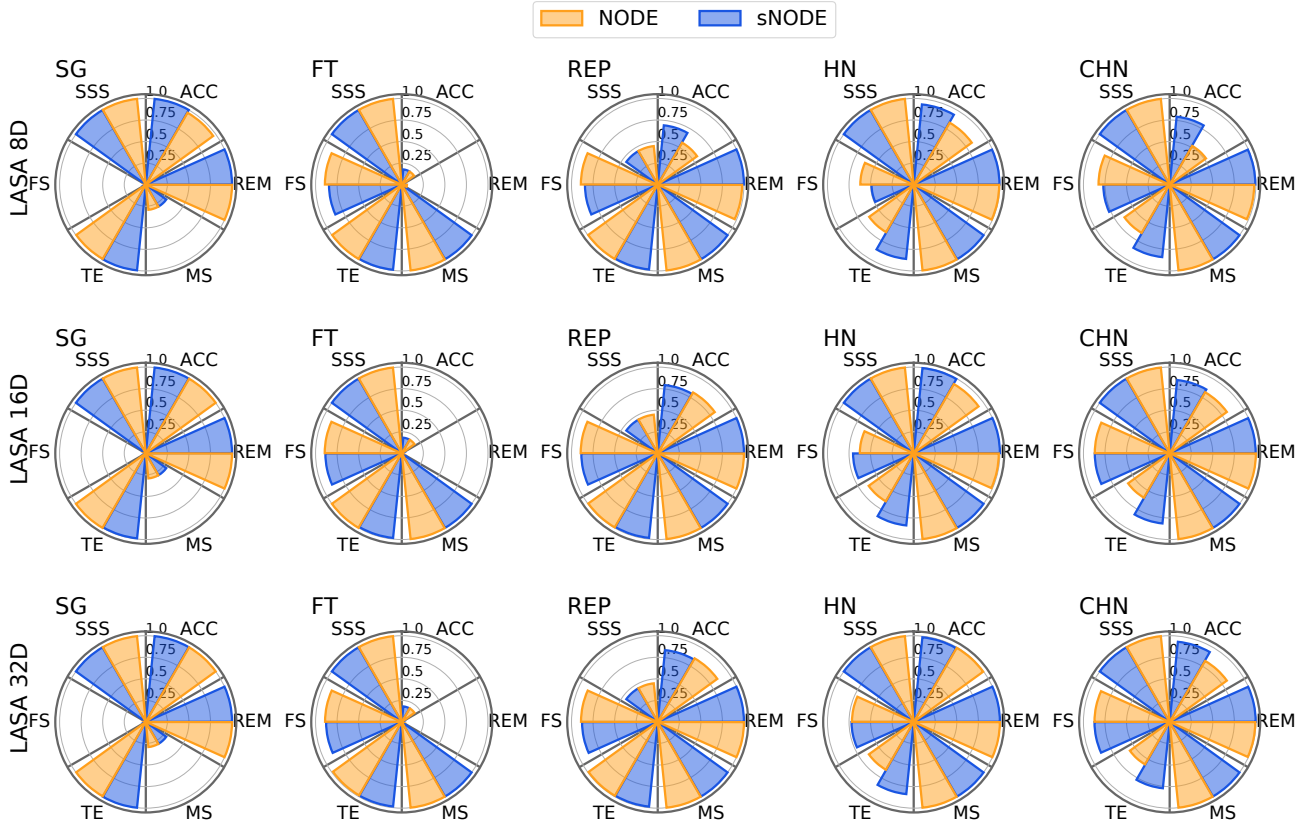


Fig. A.26. Continual learning metrics (0:worst-1:best) for SG, FT, REP, HN, and CHN for the high-dimensional LASA datasets. The scores for both task learners (NODE and sNODE) are shown. The use of sNODE improves the continual learning performance of CHN, which achieves the best overall continual learning performance (see Tab. A.3 for overall CL scores).

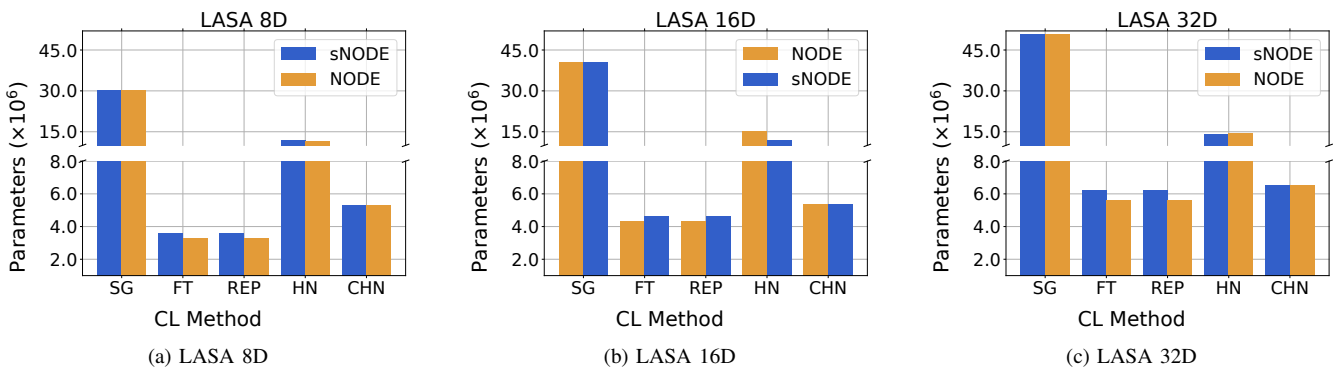


Fig. A.27. Model parameter counts after learning all 10 tasks of the high-dimensional LASA datasets.

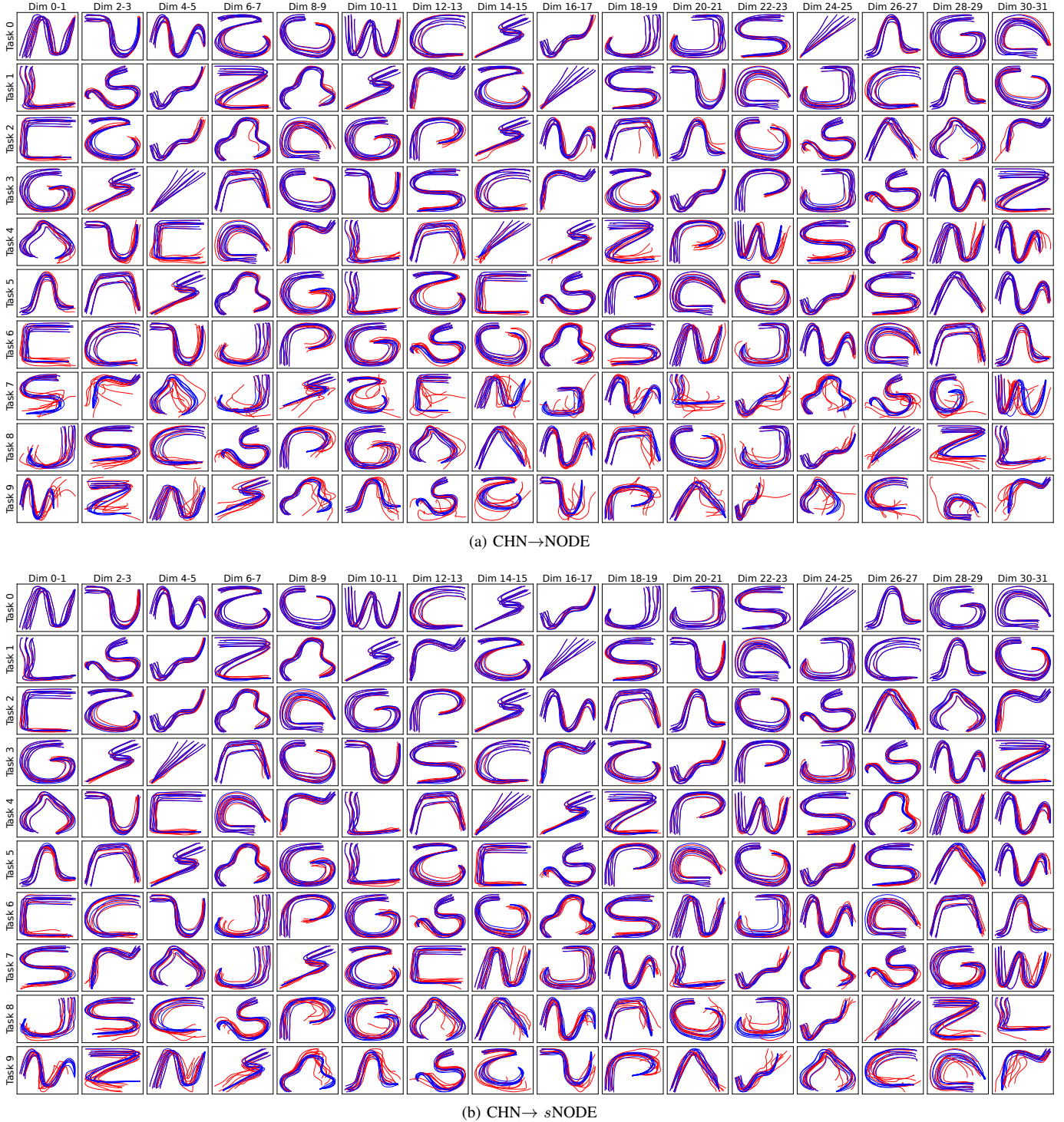


Fig. A.28. Qualitative examples of predictions produced by (a) CHN→NODE and (b) CHN→sNODE for the 10 tasks of the LASA 32D dataset after learning all tasks. The ground truth is shown in blue, and predictions are shown in red. In both (a) and (b), each row represents a single task. Each column shows the 32 dimensions of a task by grouping 2 consecutive dimensions together. Overall, CHN→sNODE produces much fewer erroneous predictions than CHN→NODE.

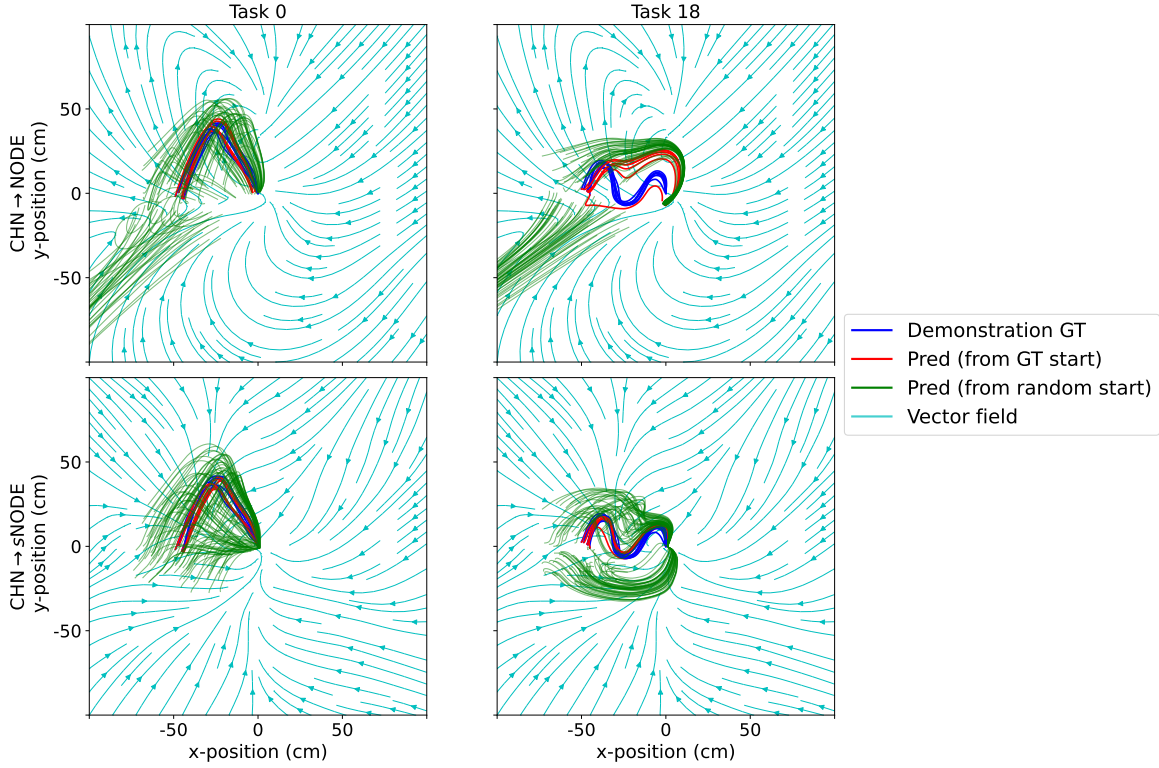


Fig. A.29. Qualitative examples of predictions produced by (a) CHN→NODE, and (b) CHN→*s*NODE for a task from $\mathcal{D}_{\text{LASA2D}}$, where the starting position is set randomly from a circle of radius 25 cm around the ground truth starting position. Ground truth demonstrations are shown in blue, predictions produced when starting from the ground truth starting position are shown in red, and predictions for random starting positions are shown in green. Even when starting at a position very different to that of the demonstration, the trajectories predicted by CHN→*s*NODE still converge near the goal, while CHN→NODE exhibits severe divergence. Since both models learn a time-dependant vector field, the streamlines in the plot depict the vector field in the final timestep of the trajectory.

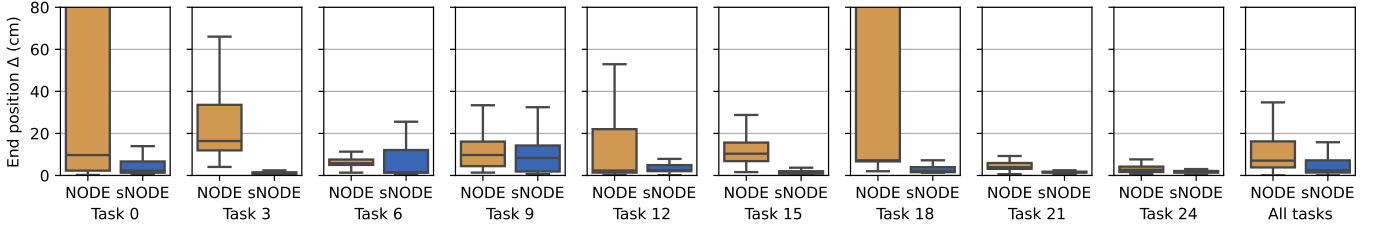


Fig. A.30. Quantitative results of the stability analysis of CHN→NODE and CHN→*s*NODE on $\mathcal{D}_{\text{LASA2D}}$. For each task, the starting position is set randomly from a circle of radius 25 cm around the ground truth starting position, and we measure the distance between the ground truth goal and the end point of the predicted trajectory (goal Δ). (a) CHN→NODE shows divergence for multiple tasks, but CHN→*s*NODE converges near or at the goal. (b) The overall goal Δ for CHN→*s*NODE is much better than CHN→NODE.

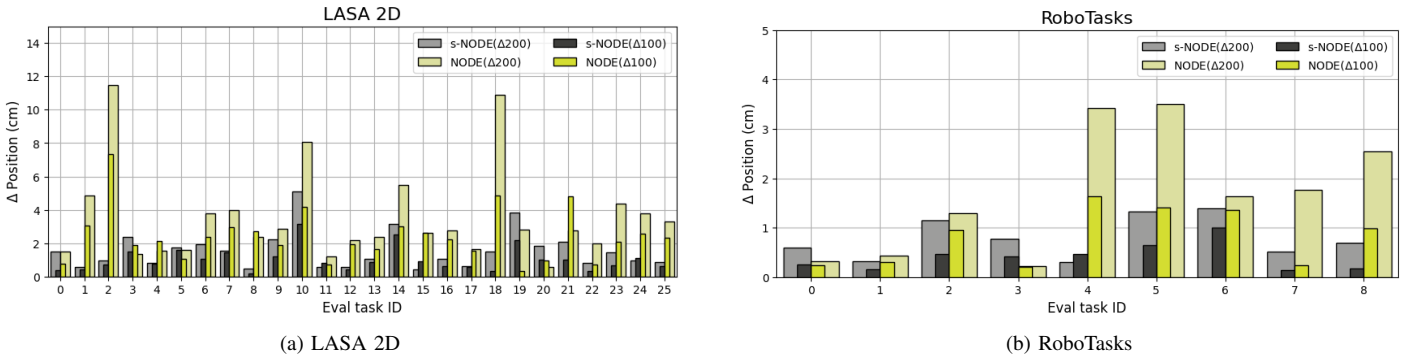


Fig. A.31. We make CHN→NODE and CHN→*s*NODE predict trajectories of 1100 and 1200 steps (the models were trained on ground truth demonstrations of 1000 steps) and we measure goal Δ , that is the distance between the ground truth goal and the end point of the predicted trajectories. The goal Δ for CHN→*s*NODE is much lower than CHN→NODE for both (a) LASA 2D, and (b) Robotasks9 datasets.

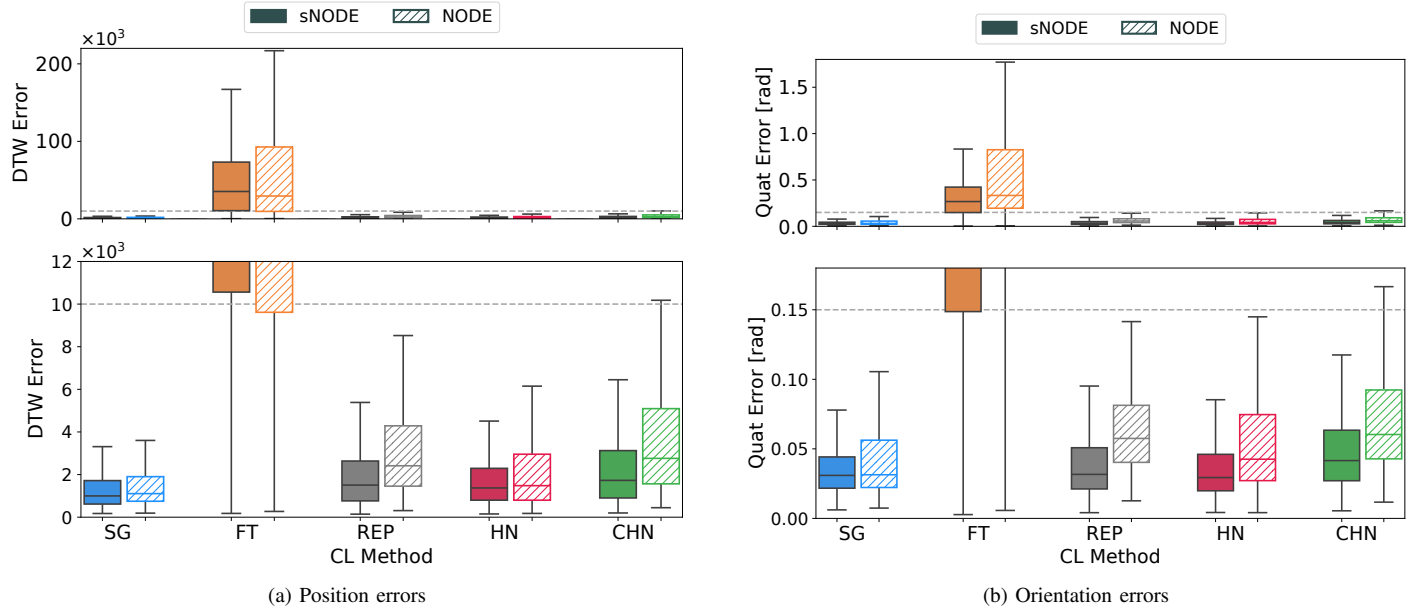


Fig. A.32. Position and orientation errors for RoboTasks9, including FT.

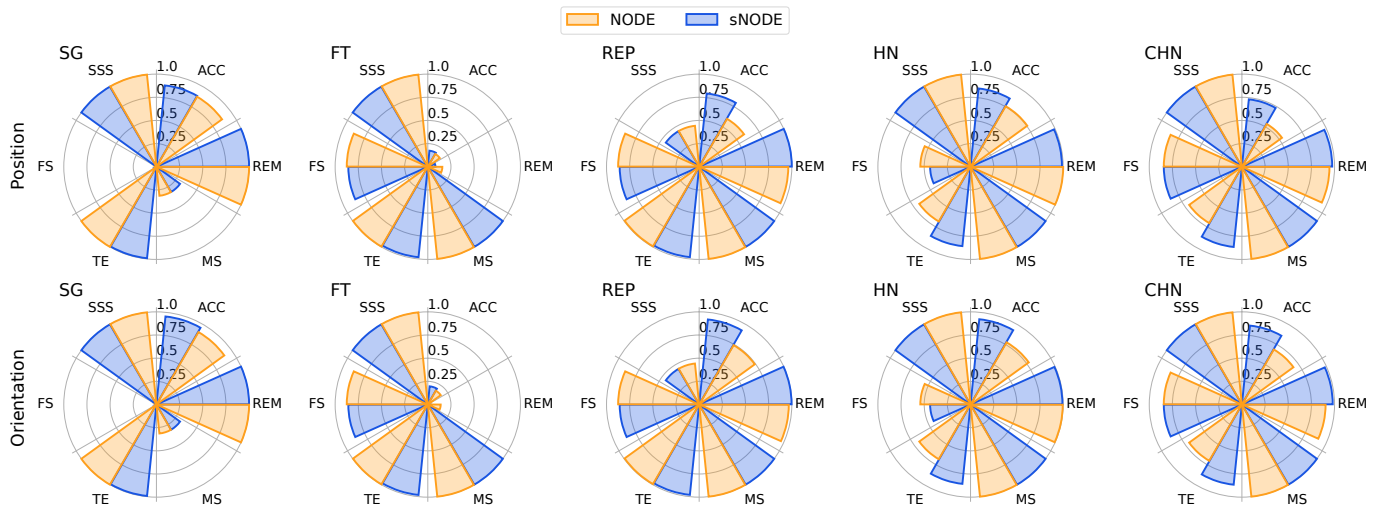


Fig. A.33. sNODE improves continual learning: Continual learning metrics (0:worst-1:best) for SG, FT, REP, HN, and CHN for the RoboTasks9 dataset. The scores for both task learners (NODE and sNODE) are shown. The top and bottom rows show the CL metrics derived from the position and orientation errors respectively. The use of sNODE improves the continual learning performance of REP, HN and particularly that of CHN, which achieves the best overall continual learning performance.

MET	ACC	REM	MS	TE	FS	SSS	CL _{sco}	CL _{stab}
SG	0.96	1.00	0.29	1.00	0.00	1.00	0.71	0.55
FT	0.18	0.06	1.00	1.00	0.89	1.00	0.69	0.56
REP	0.56	0.98	1.00	1.00	0.89	0.45	0.81	0.76
HN	0.83	0.99	1.00	0.64	0.62	1.00	0.85	0.82
CHN	0.52	0.98	1.00	0.65	0.82	1.00	0.83	0.80

(a) LASA 8D NODE

MET	ACC	REM	MS	TE	FS	SSS	CL _{sco}	CL _{stab}
SG	1.00	1.00	0.29	1.00	0.00	1.00	0.72	0.55
FT	0.18	0.04	1.00	0.99	0.84	1.00	0.68	0.55
REP	0.69	1.00	1.00	0.99	0.84	0.45	0.83	0.78
HN	0.94	0.99	1.00	0.87	0.49	1.00	0.88	0.80
CHN	0.79	0.99	1.00	0.84	0.77	1.00	0.90	0.89

(b) LASA 8D sNODE

MET	ACC	REM	MS	TE	FS	SSS	CL _{sco}	CL _{stab}
SG	1.00	1.00	0.29	1.00	0.00	1.00	0.72	0.55
FT	0.18	0.00	1.00	1.00	0.89	1.00	0.68	0.54
REP	0.82	1.00	1.00	0.99	0.89	0.45	0.86	0.79
HN	0.93	0.99	1.00	0.64	0.62	1.00	0.86	0.82
CHN	0.82	1.00	1.00	0.59	0.87	1.00	0.88	0.84

(c) LASA 16D NODE

MET	ACC	REM	MS	TE	FS	SSS	CL _{sco}	CL _{stab}
SG	1.00	1.00	0.29	0.99	0.00	1.00	0.71	0.55
FT	0.18	0.00	1.00	0.99	0.89	1.00	0.68	0.54
REP	0.80	1.00	1.00	0.99	0.89	0.45	0.85	0.79
HN	0.99	1.00	1.00	0.84	0.70	1.00	0.92	0.88
CHN	0.85	1.00	1.00	0.82	0.87	1.00	0.92	0.91

(d) LASA 16D sNODE

MET	ACC	REM	MS	TE	FS	SSS	CL _{sco}	CL _{stab}
SG	1.00	1.00	0.29	1.00	0.00	1.00	0.71	0.55
FT	0.18	0.00	1.00	0.98	0.89	1.00	0.68	0.54
REP	0.85	1.00	1.00	0.99	0.89	0.45	0.86	0.79
HN	0.99	1.00	1.00	0.64	0.72	1.00	0.89	0.83
CHN	0.82	0.99	1.00	0.57	0.87	1.00	0.88	0.83

(e) LASA 32D NODE

MET	ACC	REM	MS	TE	FS	SSS	CL _{sco}	CL _{stab}
SG	1.00	1.00	0.29	1.00	0.00	1.00	0.72	0.55
FT	0.18	0.01	1.00	0.99	0.88	1.00	0.68	0.55
REP	0.84	1.00	1.00	0.99	0.88	0.45	0.86	0.79
HN	0.99	1.00	1.00	0.84	0.72	1.00	0.92	0.88
CHN	0.93	1.00	1.00	0.77	0.87	1.00	0.93	0.91

(f) LASA 32D sNODE

TABLE A.3

CONTINUAL LEARNING METRICS FOR THE HIGH-DIMENSIONAL LASA DATASETS (MEDIAN OVER 5 SEEDS). VALUES RANGE FROM 0 (WORST) TO 1 (BEST).

MET	ACC	REM	MS	TE	FS	SSS	CL _{sco}	CL _{stab}
SG	0.87	1.00	0.31	1.00	0.00	1.00	0.70	0.57
FT	0.16	0.16	1.00	1.00	0.87	1.00	0.70	0.58
REP	0.60	0.96	1.00	0.99	0.87	0.44	0.81	0.77
HN	0.76	1.00	1.00	0.68	0.54	1.00	0.83	0.80
CHN	0.53	0.95	1.00	0.70	0.84	1.00	0.84	0.81

(a) NODE

MET	ACC	REM	MS	TE	FS	SSS	CL _{sco}	CL _{stab}
SG	0.88	1.00	0.31	0.99	0.00	1.00	0.70	0.57
FT	0.17	0.08	1.00	0.98	0.86	1.00	0.68	0.57
REP	0.80	1.00	1.00	0.98	0.86	0.44	0.85	0.79
HN	0.85	0.99	1.00	0.86	0.44	1.00	0.86	0.78
CHN	0.73	0.97	1.00	0.87	0.84	1.00	0.90	0.89

(b) sNODE

TABLE A.4

CONTINUAL LEARNING METRICS FOR THE POSITION TRAJECTORIES OF THE ROBOTASKS DATASET (MEDIAN OVER 5 SEEDS). VALUES RANGE FROM 0 (WORST) TO 1 (BEST).

MET	ACC	REM	MS	TE	FS	SSS	CL _{sco}	CL _{stab}
SG	0.90	1.00	0.31	1.00	0.00	1.00	0.70	0.56
FT	0.17	0.14	1.00	1.00	0.87	1.00	0.70	0.58
REP	0.74	0.97	1.00	0.99	0.87	0.44	0.84	0.78
HN	0.78	1.00	1.00	0.68	0.54	1.00	0.83	0.80
CHN	0.69	0.90	1.00	0.70	0.84	1.00	0.86	0.86

(a) NODE

MET	ACC	REM	MS	TE	FS	SSS	CL _{sco}	CL _{stab}
SG	0.96	1.00	0.31	0.99	0.00	1.00	0.71	0.56
FT	0.20	0.01	1.00	0.98	0.86	1.00	0.67	0.55
REP	0.92	1.00	1.00	0.98	0.86	0.44	0.87	0.79
HN	0.92	0.99	1.00	0.86	0.44	1.00	0.87	0.78
CHN	0.86	0.98	1.00	0.87	0.84	1.00	0.92	0.92

(b) sNODE

TABLE A.5

CONTINUAL LEARNING METRICS FOR THE ORIENTATION TRAJECTORIES OF THE ROBOTASKS DATASET (MEDIAN OVER 5 SEEDS). VALUES RANGE FROM 0 (WORST) TO 1 (BEST).